UiT
THE ARCTIC
UNIVERSITY
OF NORWAY

Faculty of Science and Technology
Department of Physics and Technology

The Future of Solar Energy in Marine Applications

Sigurd Dahlen

EOM-3901 Master's Thesis in Energy, Climate and Environment, 30 sp - June 2018

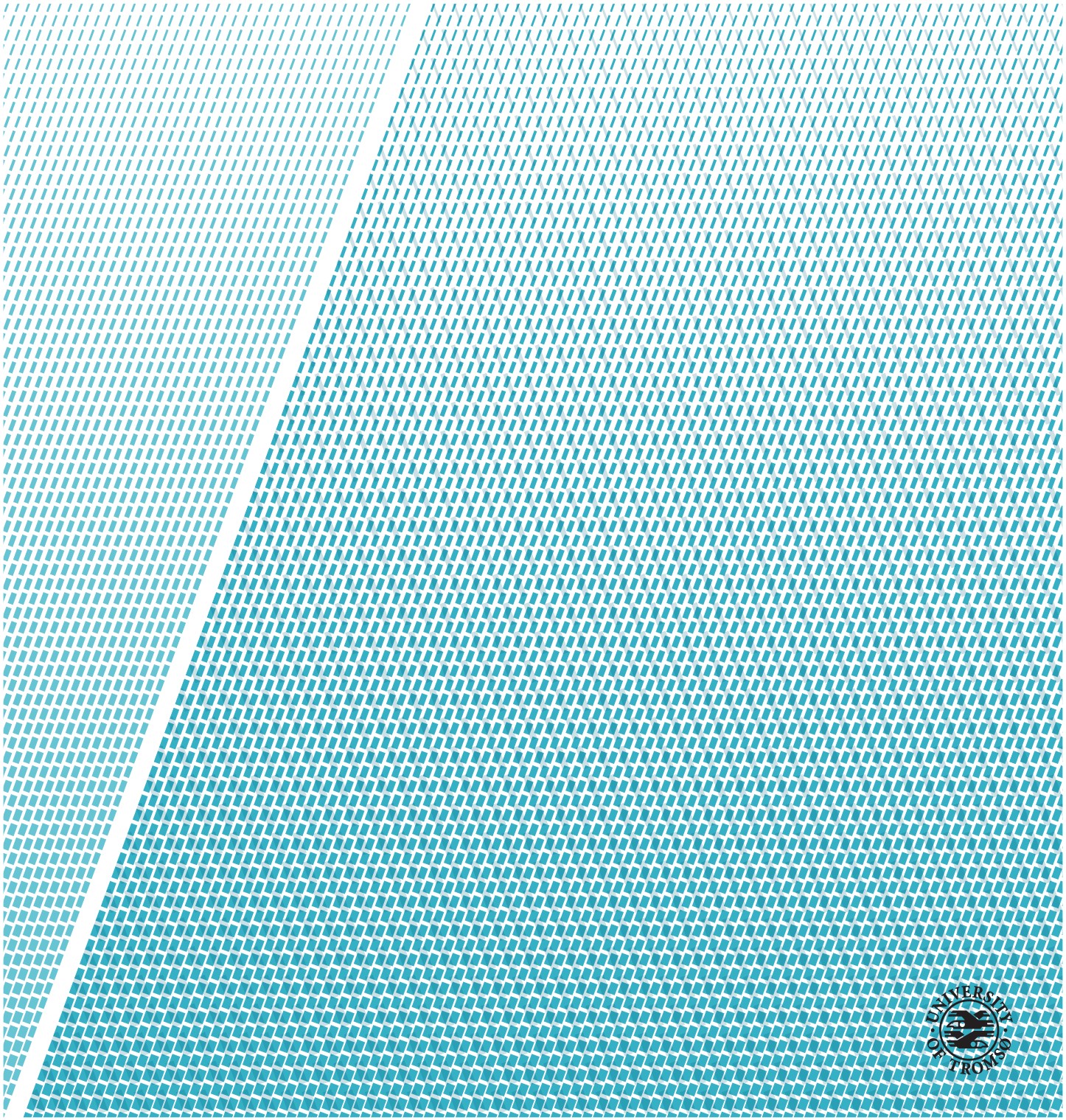

Abstract

The objective of this master's thesis is to investigate the current and future technical and economic feasibility of PV systems for marine applications. Two scenarios will be studied; a land-based PV power station to supply an in-land ferry in Norway and a PV system installed on a wind farm support vessel as a supplementary power source. The two scenarios are use cases that support the two research programmes ENERGIX and NEXUS, where Rolls-Royce Marine are participants. The simulation software *PVsyst* will be utilized in detail to perform computational simulations of different vessels, with focus on Key Performance Indicators, such as average produced energy per square meter given a certain operational area in the world. In addition, *PVsyst* will be used to perform an economic analysis.

The results show that the land-based PV power station has an annual average energy production of 132 kWh/m^2. It produces 2 046 MWh/year, which equals 110 % of MF Amperes annual consumption. The energy cost from the system will be 1.25 NOK/kWh. The PV system on the wind farm support vessel, Edda Passat, has an annual average energy production of 173 kWh/m^2. This corresponds to a production of 87.9 MWh/year, which accounts for 2.86 % of Edda Passats annual consumption. The energy cost for this system will be 0.5 NOK/kWh. The land-based system and the system on Edda Passat is estimated to have an energy payback time of 2.5 and 2 years, respectively. In addition, the life-cycle analysis emissions could be reduced by 90-95 % by using power from solar PV instead of oil and gas. The future potential of solar PV is promising with an expected increase in efficiency of 26.4 % for monocrystalline Si-cells over the next 10 years, and a predicted total system cost reduction of 53 % by 2025. Based on this, the land-based system could produce 2 587 MWh/year with an energy cost of 0.59 NOK/kWh, and the system on Edda Passat could produce 111 MWh/year with an energy cost of 0.24 NOK/kWh by 2028. The future energy cost from the PV system on Edda Passat and the land-based system corresponds to 12 % and 30 % of present marine gas oil costs, respectively. Solar modules have a lifetime of at least 25 years and are classified for use in marine environments by the International Electrotechnical Commission. These numbers show that solar PV is an important part of power generation for future solutions in marine applications.

Acknowledgements

First of all, I would like to thank Hans Martin Hjørungnes, Kristian Eikeland Holmefjord and Sigurd Øvrebø for giving me the opportunity to work on this project in collaboration with Rolls-Royce Marine. A special thanks to my co-supervisor, Kristian Eikeland Holmefjord, for providing me with important data, great advice and for answering my questions at all times. I am also grateful for good and encouraging discussions with Sigurd Øvrebø.

I would also like to thank my supervisor, Tobias Boström, for help, discussions and feedback. I am also grateful for help and advice regarding simulations in *PVsyst* from Clara Good.

A special thanks to Karl-Fredrik Hansen, whom I shared office with, for all discussions, coffee breaks and laughs. I would also like to thank Benjamin Shaver for proofreading. Thanks to my fellow students for five amazing years. I appreciate all the good memories and friendships made during these five years.

Finally, I want to express gratitude to my family for all the support throughout the five years, and especially through the last semester.

Contents

List of Figures

List of Tables

Abbreviations

AC Alternating current

AM Air mass

BEP Break-even point

BoS Balance of System

BSF Back Surface Field

DC Direct current

EPBT Energy payback time

GABP Global average bunker price

GWA Global weighted average

IEC International Electrotechnical Comission

IMO International Maritime Organization

ITRPV International Technology Roadmap for Photovoltaic

KPI Key Performance Indicators

LCA Life-cycle analysis

LNG Liquefied Natural Gas

NASA National Aeronautics and Space Administration

NTA The Norwegian Tax Administration

MGO Marine gas oil

mt Metric tonnes

PERC Passivated emitter rear cell

PERL Passivated emitter rear locally diffused

PERT Passivated emitter rear totally diffused

PV Photovoltaic

SHJ Silicon heterojunction

SSE Surface Meteorology and Solar Energy programme

tkm Tonne-kilometre

toe Tonnes of oil equivalent

Nomenclature

The symbols listed below are sorted alphabetically with the Latin symbols first, followed by the Greek symbols.

Symbol	Description	Unit
A_A	Weather deck area on MF Ampere	m^2
A_{EP}	Weather deck area on Edda Passat	m^2
B	Breadth	m
I	Current	A
I_m	Maximum current	A
I_{SC}	Short-circuit current	A
I_o	Dark saturation current	A
k	Boltzman constant	$1.381 \cdot 10^{-23}$ J/K
m	Mass	kg
N	Ratio of actual area to circumscribed rectangular	
P_m	Maximum power point	W
P_{rad}	Solar radiation power	W
q	Electron charge	$1.602 \cdot 10^{-19}$ C
t	Time	s
T	Temperature	K
T_H	Difference of highest ambient temperature from STC	°C
T_L	Difference of lowest ambient temperature from STC	°C
V	Voltage	V
V_{HI}	Maximum acceptable inverter voltage	V
V_{HM}	Highest expected module voltage	V
V_{LI}	Minimum acceptable inverter voltage	V
V_{LM}	Lowest expected module voltage	V
V_m	Maximum voltage	V
x	Position	m
X	Path length overhead	m
Y	Path length	m

Symbol	Description	Unit
β	Tilt angle	degrees
η	Efficiency	%
θ_{M}	Module incidence angle	degrees
θ_{S}	Surface incidence angle	degrees
θ_{Z}	Zenith angle	degrees
κ	Wave number	rad/m
ν	Frequency	Hz
ξ	Surface profile	
ξ_0	Amplitude	m
Φ	Incident radiation module	$\mathrm{W/m^2}$
Φ_{m}	Measured direct radiation module	$\mathrm{W/m^2}$
ω	Angular frequency	rad/s

1 Introduction

The rapid development in solar module technology has allowed solar energy integration in many applications previously deemed uneconomical. They are an environmental friendly alternative to any type of carbon-combustion system and have the potential to be a game changer in several industries. Over the last decades, the price of solar modules have decreased tremendously while the efficiency has increased significantly. PV modules have experienced a cost reduction of more than 80 % from the end of 2010 to 2017 [IRENA, 2018], while the efficiency has increased by over 40 %, from about 12 % to 17 %, over the last 10 years for average commercial wafer-based silicon modules (above 20% efficiency for super-mono modules) [Fraunhofer ISE, 2017]. With this, solar modules have definitely made their entry in most of the transport sectors, including the maritime sector. According to the International Maritime Organization (IMO), maritime transport were responsible for about 2.5 % of global greenhouse gas emissions in 2011 [Smith et al., 2015]. This amount could be greatly reduced by converting to electric propulsion systems combined with photovoltaic modules for additional power generation.

This thesis is written in collaboration with *Rolls-Royce Marine AS*, who wants to look further into the use of PV modules in marine applications. Rolls-Royce Marine has a very broad product range, and over 30,000 commercial vessels around the world use their equipment [Rolls-Royce plc, 2018]. Among their products, one can find hybrid and electrical propulsion systems and battery packages [Rolls-Royce plc, 2017b]. These systems can be combined with renewable energy sources, such as PV modules, in order to generate zero-

emission power for the hybrid/electric propulsion systems. By combining these systems, one can reduce fuel usage, greenhouse gas emissions, and costs related to fuel and taxes for emitting greenhouse gases.

Rolls-Royce participates in the European research and development project NEXUS, whose goal is to develop new service operation vessel designs and business concept to meet the rapidly growing need for wind farm support vessels [ARTTIC, 2018]. Whereas Rolls-Royce collaborates with ENERGIX for the project regarding fully electric ferries in Norway. ENERGIX is a programme for research on renewable energy, energy systems, efficient use of energy, and energy policy funded by The Research Council of Norway and Enova [Enova, 2018c] [The Research Council of Norway, 2018].

1.1 Objective

This master's thesis will investigate the current and future technical and economic feasibility of using solar panels for marine applications, either on-board a vessel or as land-based support. A description of solar modules and marine vessels will be the introduction to the thesis. An investigation of the technical possibilities and limitations of solar panels will lay the groundwork for a detailed study, including simulations of the energy created utilizing solar modules on-board a wind farm support vessel. The study will also focus on simulations of produced power from a land-based PV power station.

For wind farm support vessels the PV modules are an interesting field of study as a supplementary power source, while inland ferries in Norway could perhaps only be supported by power generated from PV modules installed on the ferry and/or on land. The performance of solar panels on marine vessels will be influenced by many factors like vessel motions, heading, geographical area, environmental contamination, etc.

The simulation software *PVsyst* will be utilized in detail to perform computational simulations of different vessels, with focus on Key Performance Indicators (KPI's), such as average produced energy per square meter and specific energy production, given a certain operational area in the world. The main result of the thesis gives an estimation of the current energy payback time, emission-reduction, and efficiencies of solar panels in marine application and provides a predicted indication of the future economic and technological development within solar modules for marine applications.

1.2 Structure of the Thesis

The thesis contains the following chapters, excluding introduction:

Chapter 2 presents information about greenhouse gas emissions in the maritime sector, and growth and cost of solar modules. In addition, it contains theory about solar modules and important parameters for power production from solar modules. It also comprises of theory about batteries, converters, and the oceans motion.

Chapter 3 introduces the economical aspects concerning operation and maintenance of PV systems, fuel and greenhouse gas emission taxes. Cost reduction potentials of PV modules is also included.

Chapter 4 describes vessel design and the geographical location of operation for the vessels.

Chapter 5 introduces how the simulation software works, and what type of PV modules that will be used for simulation. The simulation scenarios and potential evolution of PV in marine applications will also be presented.

Chapter 6 presents the results obtained from simulations for the power station at Lavik, and for the PV system integrated on Edda Passat. The results are then discussed.

Chapter 7 provides a summary of the most important results, and includes suggestions for future work.

2 Theory

This chapter includes information about greenhouse gas emissions in the maritime sector, and growth and cost of solar modules. In addition, it contains theory about solar modules and important parameters for power production from solar modules. It also comprises of theory about batteries, converters, and the oceans motion.

2.1 Global and Maritime CO_2 Emissions

The marine industry transports around 90 % of global trade [IMO, 2011]. These goods include raw materials, consumer goods, food, and energy, and according to the International Maritime Organization (IMO) there are no better way of transporting goods around the world in means of efficiency, safety, and environmental friendliness. For marine transport, CO_2 emissions per tonne-kilometre (tkm)[1] are 31 gCO_2/tkm, while airfreight emits 602 gCO_2/tkm and road transport has an emission of 62 gCO_2/tkm [Cefic & ECTA, 2011]. Hence, the transportation of goods by aircraft and lorries emits 20 and 2 times as much CO_2 as transportation by ships, respectively. However, the global marine industry accounted for only 3.1 % of annual global CO_2 emissions, in average, during the period 2007 – 2012 , as seen in Table 2.1 [Smith et al., 2015]. Ferries

1. A tonne-kilometre is a unit of measure which represents the transport of one tonne of goods over one kilometre.

and wind farm support vessels are also a part of the numbers to be presented, but will not be focused on due to lack of precise data.

Table 2.1: Global shipping CO_2 emissions compared with global CO_2 emissions, values in million tonnes CO_2 [Smith et al., 2015].

Year	Global CO_2	Total shipping	% of global	International shipping	% of global
2007	31,409	1,100	3.5 %	885	2.8 %
2008	32,204	1,135	3.5 %	921	2.9 %
2009	32,047	978	3.1 %	855	2.7 %
2010	33,612	915	2.7 %	771	2.3 %
2011	34,723	1,022	2.9 %	850	2.4 %
2012	35,640	938	2.6 %	796	2.2 %
Average	33,273	1,015	3.1 %	846	2.6 %

Table 2.1 illustrates global[2], total shipping, and international shipping CO_2 emissions from 2007 – 2012. In addition, it shows CO_2 emissions from total shipping and international shipping as a percentage of global CO_2 emissions. During this period, the total shipping CO_2 emissions declined due to a reduction in emissions in the oil tanker sector, bulk carrier sector, and container ship sector. The oil tanker sector reduced its total fleet's CO_2 emissions by over 20 %, while the bulk carrier sector experienced approximately a 5 % reduction and the container ship sector reduced their emissions by 1 – 2%, as illustrated in figures A.4-A.6 in Appendix A. In addition, these three sectors have also been able to reduce the fleet transport work CO_2 intensity while increasing the total installed power of the fleet, demand tonne-miles, and total deadweight tonnage fleet capacity, as seen in figures A.4-A.6.

The main reason for the reduction in CO_2 emissions is due to the decrease in average days at sea and the ratio of average at sea speed to design speed, as illustrated in figures A.1-A.3 in Appendix A. Figure A.1 shows a decrease of 15 % in average days at sea and ratio of average at sea speed to design speed for the oil tanker sector during the period 2007 – 2012. The average trends in the bulk carrier sector from 2007 – 2012 is a 22 % decrease in average days at sea and a 12 % decrease in ratio of average at sea speed to design speed, as illustrated in Figure A.2. From Figure A.3 it is evident that the container ship sector experienced a 5 % increase in average days at sea and a reduction of the ratio of average at sea speed to design speed of 10 % during the period 2007 – 2012.

The trends in average fuel consumption per ship occur due to a reduction in both speed and days at sea [Smith et al., 2015]. This, in combination with

2. The global CO_2 emissions are based on emissions from fossil fuel burning and cement production [Smith et al., 2015].

number of ships in service, is the reason for a reduction in fleet total CO_2 emissions. Further on, the trends in speed and days at sea follow from values near a historic low in terms of productivity (transport work per unit of capacity). Consequently, number of ships in service, fleet total installed power, and demand tonne-miles have seen upward trends, but are somewhat controlled by excess supply of fleet and high fuel prices. These upward trends also leads to reduced productivity.

In 2015, the world total final consumption (TFC) of fuel were 9 384 Mtoe, including international aviation and international marine bunkers, as illustrated in Figure 2.1 [IEA, 2017]. The fuel shares in Figure 2.1 are divided in six categories: Coal [3], Oil, Natural gas, Biofuels and waste [4], Electricity and Other [5].

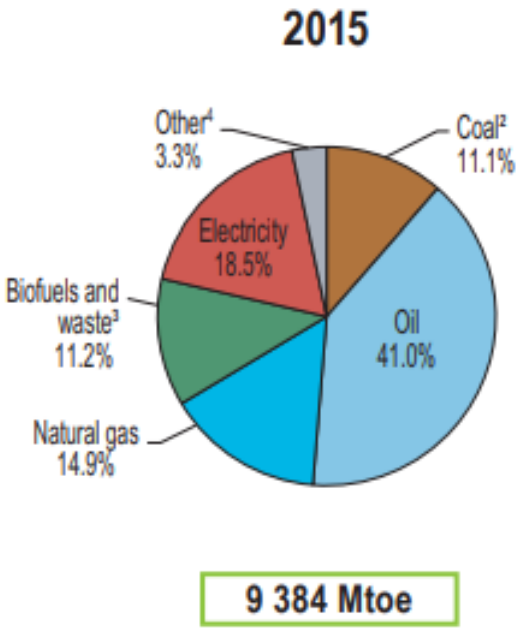

Figure 2.1: Fuel shares of total final consumption in 2015 [IEA, 2017].

Figure 2.2 shows world TFC shares of oil in 2015. From the figure it is evident that marine navigation consumes 6.7 % of TFC of oil, which corresponds to 257 Mtoe [IEA, 2017]. By using a conversion ratio of 3 223 $kgCO_2$/ tonne fuel oil, consumption by navigation sector is equal to approximately 830 million tonnes of CO_2 [Carbon Trust, 2008]. This is a reduction of over 10 % from 2012.

3. Peat and oil shale are included in this category.
4. The TFC for biofuels and waste have been estimated for a number of countries.
5. Includes heat, solar thermal and geothermal.

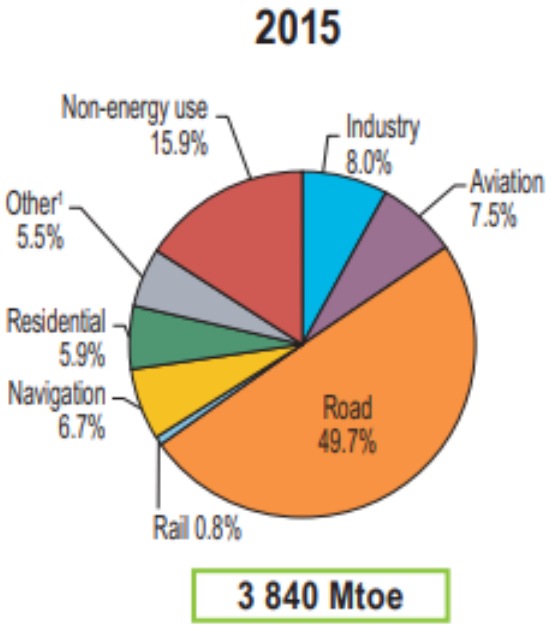

Figure 2.2: TFC shares of oil in 2015 [IEA, 2017].

2.2 Growth and Cost Trends of Solar PV

Over the last decade the global PV market has grown substantially. The cumulative global installed capacity increased from 6.1 GW at the end of 2006 to 291 GW at the end of 2016, as illustrated in Figure 2.4 [IRENA, 2018]. The installation of solar PV in European countries has declined since 2011, where the installed capacity was 22 GW, as can be seen in Figure 2.3. Europe had the highest amount of global cumulative PV capacity in 2015 with 44 %, but it decreased to 35 % at the end of 2016. In 2013, the Asian PV market had tremendous growth, with an installation of approximately 20 GW, more than doubling the amount of installed capacity from year 2012, as shown in Figure 2.3. The Asian PV market continued its growth the following years, and experienced a record-high installation of approximately 50 GW in 2016. By the end of 2016, the Asian PV market accounted for approximately 48 %, while the market in United States accounted for 11 % of the global installed cumulative capacity.

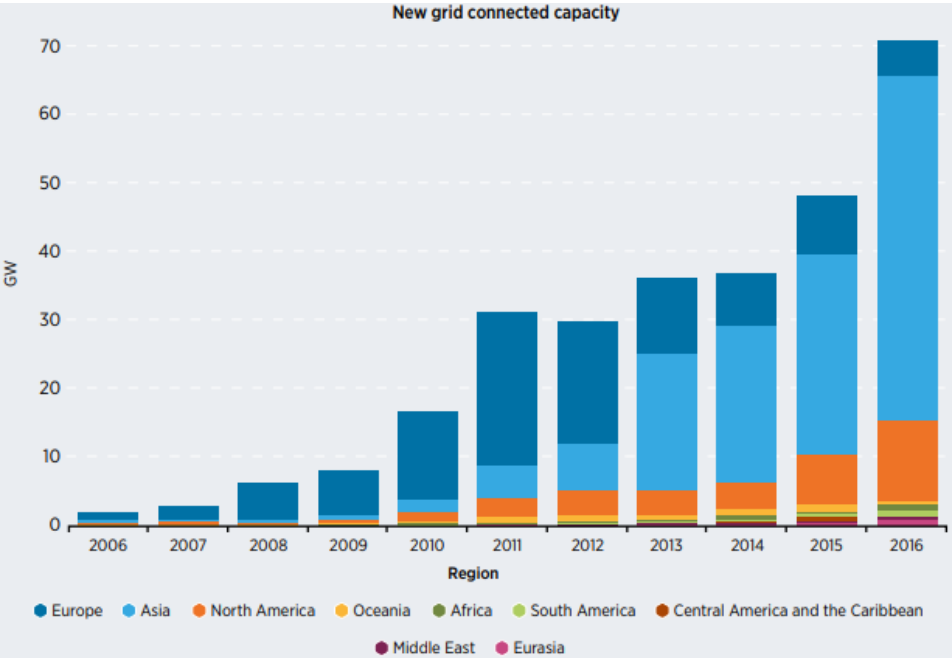

Figure 2.3: Annual installed global PV capacity by region from 2006 to 2016 [IRENA, 2018].

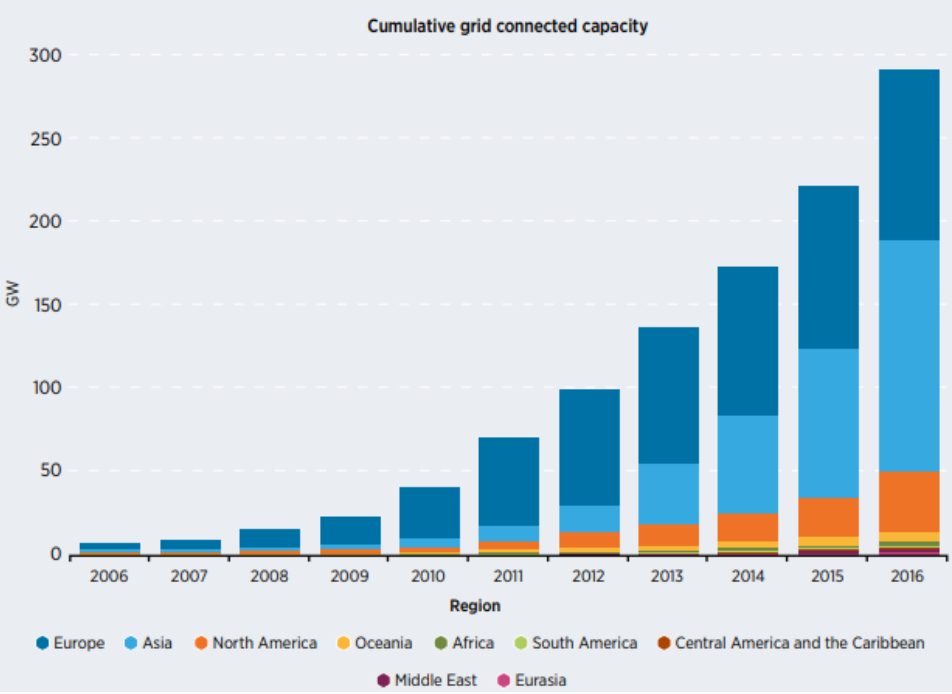

Figure 2.4: Annual cumulative global PV capacity by region from 2006 to 2016 [IRENA, 2018].

The PV module prices in Europe declined by 83 % from March 2010 to March 2017, as seen in Figure 2.5 [IRENA, 2018]. The prices for PV modules decreased rapidly until 2013, but decreased moderately during the following years. From the end of 2010 to the end of 2016, the PV module prices dropped by 80 %, and during the same period, 87 % of the cumulative global PV capacity were installed. The cost reductions are partially due to the increased installed capacity, but are mainly driven by improvements in the production process and efficiency gains through new cell design. Cost reductions due to improvements in the production process occur because of the diamond wafer cutting method. This method uses a diamond wire saw to cut the material which leads to a reduction in material losses.

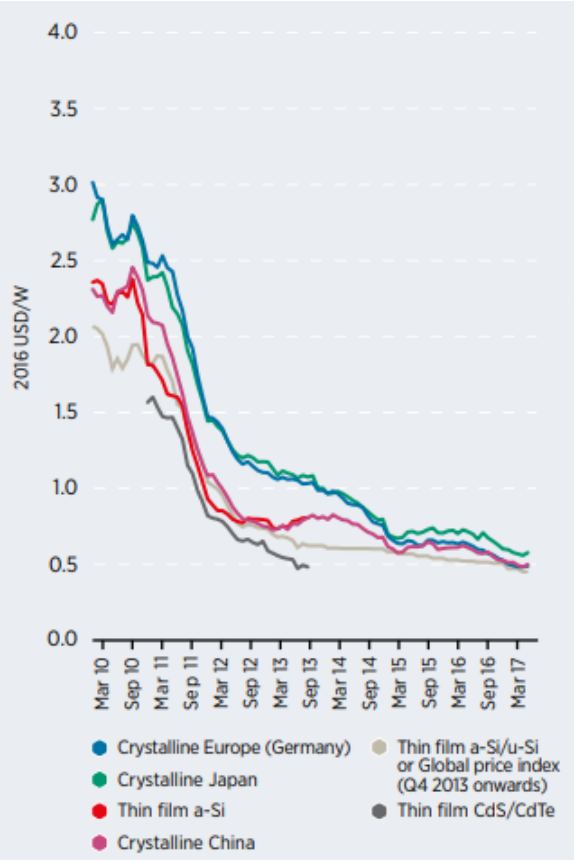

Figure 2.5: Average monthly European solar PV module prices by module technology and manufacturer from March 2010 to March 2017 [IRENA, 2018].

Total installed costs for utility-scale PV systems[6] have experienced a cost reduction due to an increasing number of cost competitive projects in India and in newer markets[IRENA, 2018]. This has led to a cost reduction of over 70 % for PV systems in many markets during the period 2010-2017, as illustrated in Figure 2.6. From 2010 to 2017, the United States experienced the lowest cost reduction at 52 %, while Italy had the highest cost reduction at 79 %.

Even though the modules and systems in this section are land-based, the cost reductions will most likely be the same for modules suitable for marine environments. However, the cost reductions for total installed costs will most likely be lower for marine applications. When installing systems on vessels, the fixing brackets should be more robust than for land-based systems, so that the system can withstand the harsh weather conditions. In addition, the need for some sort of vibration reduction for the system would be useful in order to prolong the lifetime and minimize maintenance costs. Hence the total installed costs for a PV system installed on vessels is considered to be slightly higher than for land-based systems.

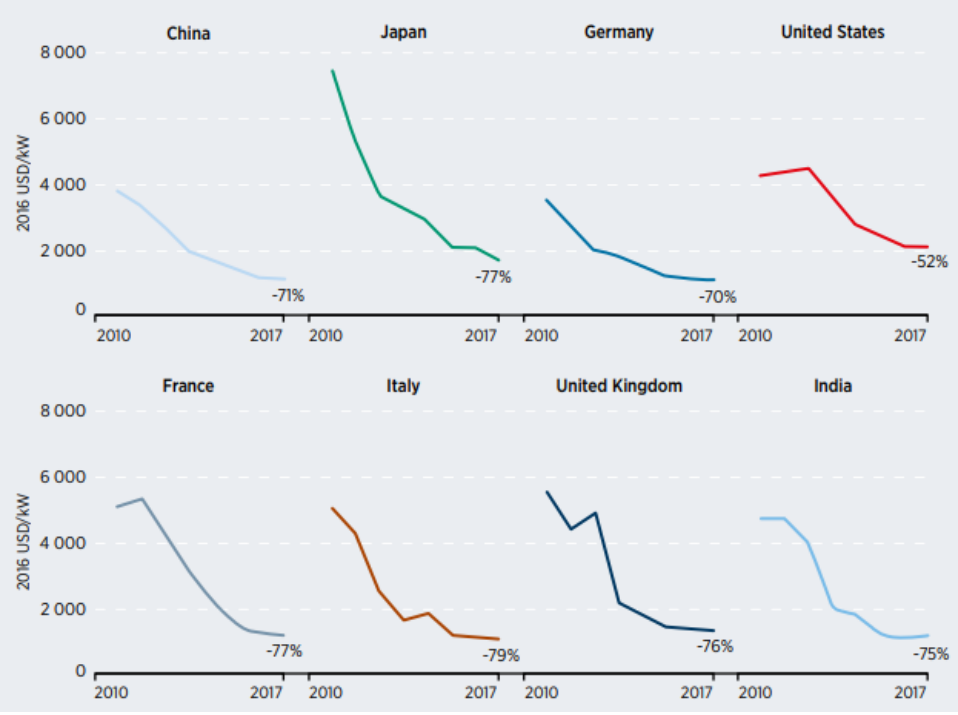

Figure 2.6: Utility-scale solar PV total installed cost trends in selected countries from 2010 to 2017 [IRENA, 2018].

6. PV systems greater than 1 MW

2.3 PV Modules and Key Parameters

A PV module is a connection of several solar cells encapsulated in a protective material [PV Education, 2018b]. The main reason for connecting solar cells into a module is to increase the power output, which can range from a couple watts to several hundred watts [Solanki, 2015]. To increase the power output even more, several PV modules can be connected into a PV array, which can achieve a power output of a few hundred watts to several megawatts.

Solar modules used in marine environment must endure harsh conditions such as strong winds, sea spray, and salty mist. The International Electrotechnical Commission (IEC) is a worldwide organisation that publishes international standards for electrical components [IEC, 2018]. When it comes to solar modules for use in marine environments, IEC has a standard named *IEC 61701*, which concerns salt mist corrosion testing of solar photovoltaic modules. Thus, solar modules with the *IEC 61701* standard are encapsulated so that the solar cells and the electrical wires are protected from rough weather conditions and salt mist, and can therefore be used in marine environments.

2.3.1 Structure of a Photovoltaic Cell

A solar cell consists of front and rear contacts, an antireflection coating, an emitter, and a base, as illustrated in Figure 2.7 [PV Education, 2017]. When solar radiation hits the solar cell, electrons gets excited and the generation of an electron-hole pair occurs. The electron will then flow in the external circuit delivering work to the load, and generate direct current (DC).

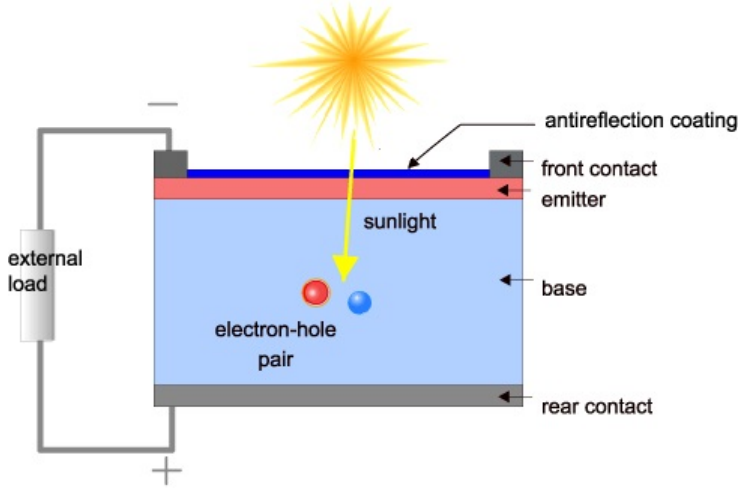

Figure 2.7: Cross section of an illuminated solar cell [PV Education, 2017]

I-V equation

The relation between current and voltage in a solar cell is shown in the I-V equation. This equation describes the current that flows through the external circuit of a PV cell under illumination [Solanki, 2015]:

$$I = I_{SC} - I_o(e^{(qV/kT)} - 1) \tag{2.1}$$

where I_o is the dark saturation current, q the electron charge, v the frequency, k the Boltzmann constant, T the temperature, and I_{SC} is the short-circuited current which is the maximum current that can flow through the solar cell. Figure 2.8 illustrates a typical I-V curve for a solar cell under illumination. From this curve, it is evident that when the terminals at P-side and N- side of the solar cell is shorted with each other, $V = 0$ and $I = I_{SC}$. To obtain maximum voltage generated, the terminals are kept open, $I = 0$ and then $V = V_{OC}$. The figure also shows a curve of the obtainable power from the solar cell, which occurs at the point I_m and V_m. Thus, the power output of the solar cell is defined as the maximum power point $P_m = I_m V_m$. The efficiency of a solar cell is defined as the ratio of power output to power input

$$\eta = \frac{P_m}{P_{rad}} \tag{2.2}$$

where the power input is the power of solar radiation P_{rad}.

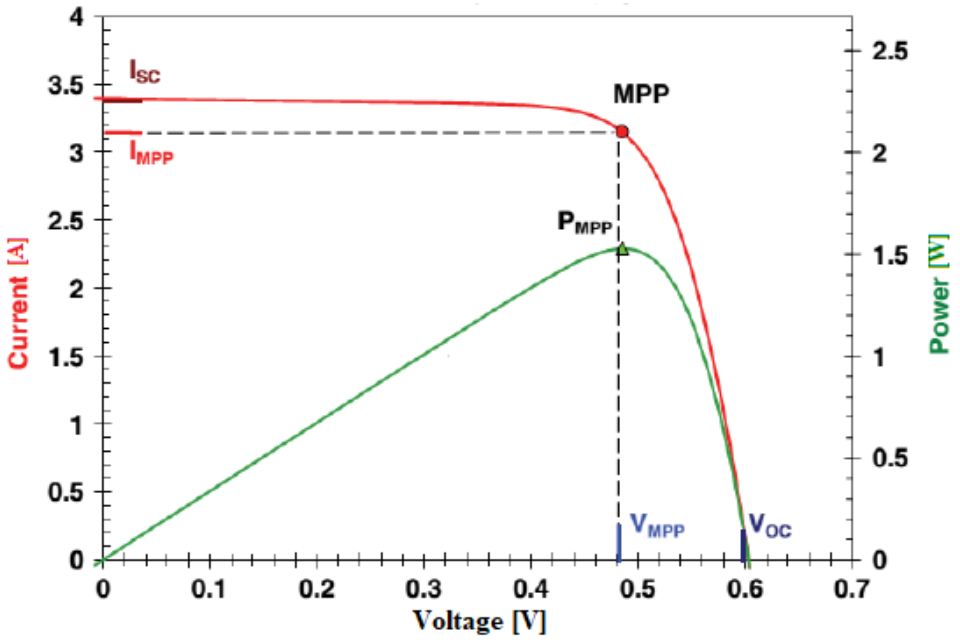

Figure 2.8: The I-V curve and power output of a solar cell under illumination [Al-Khazzar and Talib, 2015].

2.3.2 PV Technologies

Solar cell technology can be divided into two basic groups, crystalline cells and thin film cells. Crystalline cells are made out of silicon (Si), where the molecules are organized into crystalline grids, and can be divided into monocrystalline cells and polycrystalline cells [Kobougias et al., 2013]. The monocrystalline cells have a single-crystal structure, while the polycrystalline cells consists of crystal grids with different orientations. Thin film cells are made out of thin layers of photoactive semiconductors added on low-cost substrates, such as glass. The semiconductor materials are often amorphous silicon (a-Si), copper indium diselenide (CIS) and cadmium telluride (CdTe). Figure 2.9 illustrates the global annual production of PV modules by technologies, where monocrystalline accounted for approximately 24 %, polycrystalline for around 70 % and thin film for about 6 % in 2016 [Fraunhofer ISE, 2017].

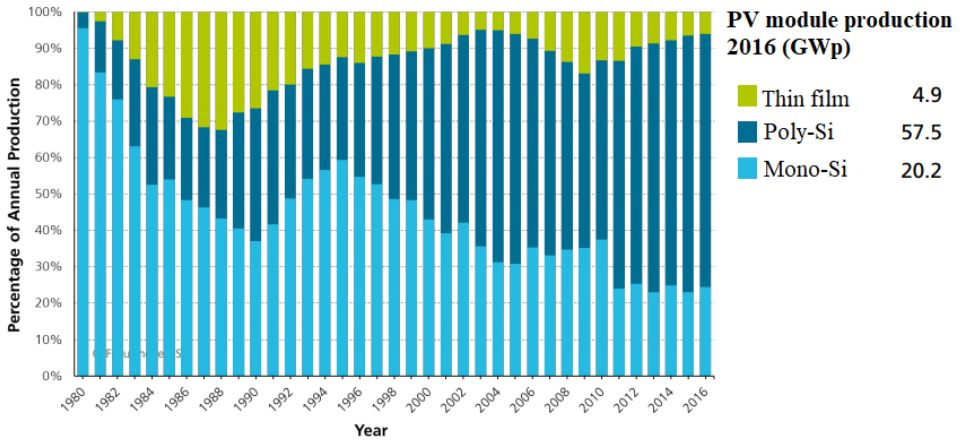

Figure 2.9: Percentage of global annual PV production by technology [Fraunhofer ISE, 2017].

Out of these three technologies, commercial monocrystalline solar cells have the highest efficiency of 15-22 %, highest power density, and an estimated lifetime of over 30 years [Fraunhofer ISE, 2017] [Kobougias et al., 2013]. The polycrystalline cells have an efficiency of 15-17% and an estimated lifetime exceeding 25 years, while the efficiency of thin film cells varies between 5-11%, with an estimated lifetime of over 20 years. However, thin film solar cells have a lower temperature coefficient than both mono- and polycrystalline cells, meaning that the efficiency decreases less for increasing temperatures. All theses technologies can be used in marine environments, but there is often limited space aboard vessels, hence, crystalline cells will be preferred due to their high efficiency and power density. Thin film cells can, however, be used for windows, railings, and transparent roof. Due to higher efficiency and longer lifetime, monocrystalline cells will be chosen over polycrystalline cells for simulations.

Solar cells can be light-sensitive on one side, monofacial, or on both sides, bifacial [ITRPV, 2018]. The most common type of cells are monofacial, but the *International Technology Roadmap for Photovoltaic (ITRPV) Results* 2017 predicts that bifacial cells will account for almost 40 % of the market by 2028. Advantages with monofacial cells are no transmittance loss of infrared light and no transmittance loss on module inactive area [Saw et al., 2017]. Disadvantages for monofacial cells are lower power output per square meter. The bifacial cells advantages' are higher power production per square meter and they are more robust due to placing between two glass surfaces [EPRI, 2016]. In addition, they are less permeable to water, which may reduce corrosion leading to a lower annual degradation rate. The additional power gain for bifacial PV modules varies from $5 - 30$ % in the field, depending on the surface. Disadvantages for bifacial cells are transmittance loss of infrared light and transmittance loss on module inactive area [Saw et al., 2017]. The price of monofacial PV modules lies around 0.5 USD/W, as illustrated in Figure 2.5, while the bifacial PV modules costs anywhere between $0.7 - 1.35$ USD/W [EPRI, 2016].

2.3.3 Path of Solar Radiation

The distance travelled by sunrays through the atmosphere normalized to the shortest possible distance through the atmosphere is called the air mass (AM) [Solanki, 2015]. At the top of earth's atmosphere, the air mass is equal to zero because the sunrays have not passed through the atmosphere yet. The radiation spectrum just outside the atmosphere is denoted as AM0 spectrum. In order to pass through the atmosphere in the shortest possible distance, the sun needs to be in the overhead position, that is, where it is at noon. The radiation spectrum at earth's surface at noon is AM1 spectrum. When the sun is in another position than the overhead position, the AM will be greater than one, and the sunrays must travel a longer distance within the atmosphere before reaching earth's surface. The greater distance travelled by the sunrays the more solar radiation will be lost through absorption interaction and scattered due to scattering interaction. Thus, the greater distance travelled by the sunrays through the atmosphere, the smaller amount of radiation hits earth's surface. The AM can be calculated by the following equation

$$AM = \frac{1}{\cos\theta_z} = \frac{Y}{X} \tag{2.3}$$

where θ_z is the angle from the vertical at a given point on the surface to the incident solar radiation, also known as the zenith angle, Y is the path length for the sun at a different position than overhead and X is the path length for

the sun in overhead position, as can be seen in Figure 2.10. For the simulations, the AM will be calculated by the simulation software *PVsyst* as it will vary with varying zenith angle.

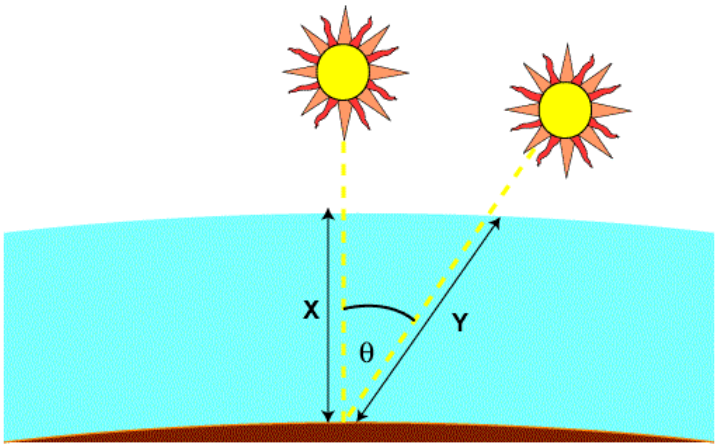

Figure 2.10: Illustrating the sun at two different positions, and the angle between their incident radiation [PV Education, 2018a].

2.3.4 Incident Radiation on PV Modules

In order to obtain maximum power density on the module, its surface should always be perpendicular to the irradiation. To obtain that, two axis tracking is required, which might be cumbersome in many situations, especially in marine applications. However, the incident radiation on a module, Φ, can be calculated by using the following equation:

$$\Phi = \Phi_m \cos\theta_M \tag{2.4}$$

where Φ_m is the measured direct radiation at an angle θ_M to the normal of the solar module [Solanki, 2015]. The incident radiation will be calculated by *PVsyst* during simulations, and will be included in the simulation report. If, however, the PV modules had one-axis or two-axis tracking, the power output could be increased by more than 30 %.

2.3.5 Surface Albedo

When solar radiation passes through the atmosphere, it will interact with different types of gaseous molecules and undergo scattering and absorption [Solanki, 2015]. The solar radiation that undergoes scattering interaction will scatter in randomly directions, in a process called diffuse radiation. A part of the solar radiation passing through the atmosphere will be absorbed by the gaseous molecules, giving the energy to the molecules, and hence lose radiation. The solar radiation that neither undergoes absorption nor scattering will reach the surface of the earth, and is called direct radiation. Once the radiation hits the surface of the earth, some of it will be reflected due to the reflection properties, albedo, of the objects on the surface and the surface itself. The albedo of an object determines how much of the solar radiation that is reflected, where an albedo of 1 leads to full reflection, and an albedo of 0 represents zero reflection (and thus full absorption). The albedo of different types of surfaces is shown in table 2.2, where θ_S is the angle between the incident radiation and the surface. Radiation reflected by surfaces on the ground is known as albedo radiation. The sum of diffuse radiation, direct radiation and albedo radiation is known as global radiation.

Table 2.2: Albedo for different types of surfaces [Quaschning, 2010].

Surface	Albedo	Surface	Albedo
Grass (Summer)	0.25	Asphalt	0.15
Lawn	0.18-0.23	Woods	0.05-0.18
Dry grass	0.28-0.32	Heathland and sand	0.10-0.25
Uncultivated fields	0.26	Water surface ($\theta_S > 45°$)	0.05
Soil	0.17	Water surface ($\theta_S > 30°$)	0.08
Gravel	0.18	Water surface ($\theta_S > 20°$)	0.12
Concrete, weathered	0.20	Water surface ($\theta_S > 10°$)	0.22
Concrete, clean	0.30	Fresh snow cover	0.80-0.90
Cement, clean	0.55	Old snow cover	0.45-0.70

For PV systems operating in snow covered areas, the incident radiation will increase due to the reflection properties of snow. Table 2.2 shows that fresh snow has an albedo of 0.80-0.90 and old snow has an albedo of 0.45-0.70. Thus, anywhere between 45 % and 90 % of the direct radiation can be reflected. This is an important aspect to consider when investigating the potential of PV systems i Norway, where there are a significant amount of snow cover days, i.e. days where snow covers the ground. The albedo for water surfaces is important to consider when installing a PV system by a lake or the sea. Depending on the angle between incident radiation and the surface of the water, anywhere between 5 % and 22 % of the incident radiation will be reflected, as shown in Table 2.2.

2.3.6 Effect of Temperature and Shading

The power output of a solar cell depends on the maximum operating current I_m and the maximum operating voltage V_m, and can be expressed as: [Solanki, 2015]:

$$P_m = I_m V_m \tag{2.5}$$

The power output of PV modules depend on the operating temperature of the cells within the modules [Solanki, 2015]. When the temperature increases, the the short circuit current increases while the open circuit voltage decreases. The decrease in open circuit voltage is considerably larger than the increase in short circuit current of the cell, as seen in figure 2.11.

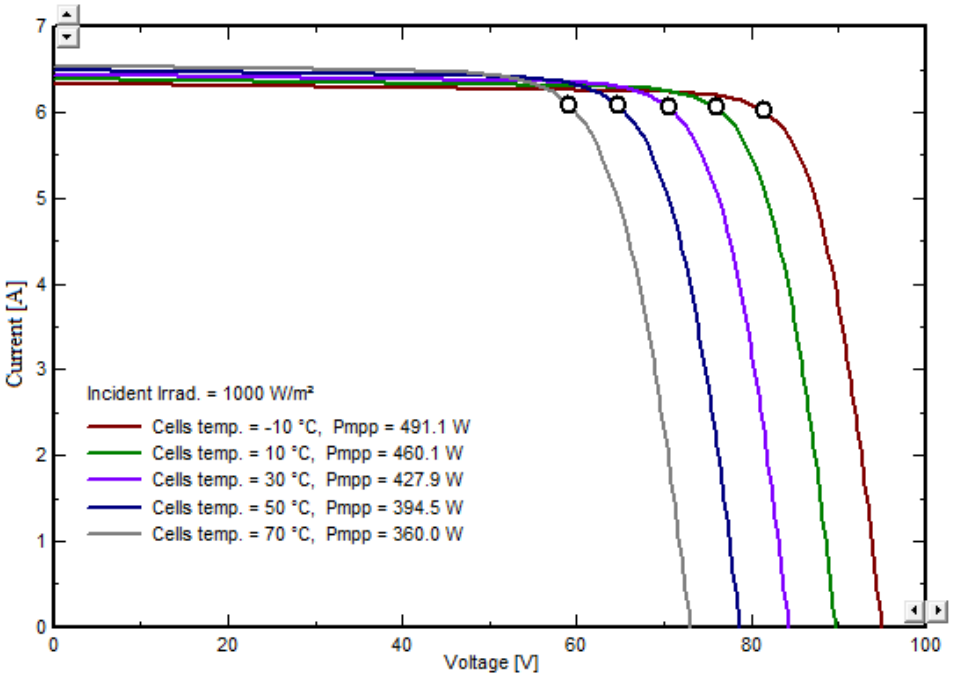

Figure 2.11: The effect of temperature on the I-V curve, and the maximum power point.

This leads to a decrease in power output from the cell, as the temperature increases, as illustrated in figure 2.12. From the figure, it is evident that a temperature increase of 20 °C corresponds to a power drop of 8 %. While a 20 °C decrease in temperature leads to an increase in power output of 7.5 %. PV modules that operate in colder environments, given that incident radiation is the same, will therefore have a higher power output than those operating in warmer environments. For PV modules installed on vessels, the high winds

at sea can contribute to ventilate the modules and hence increase the power output.

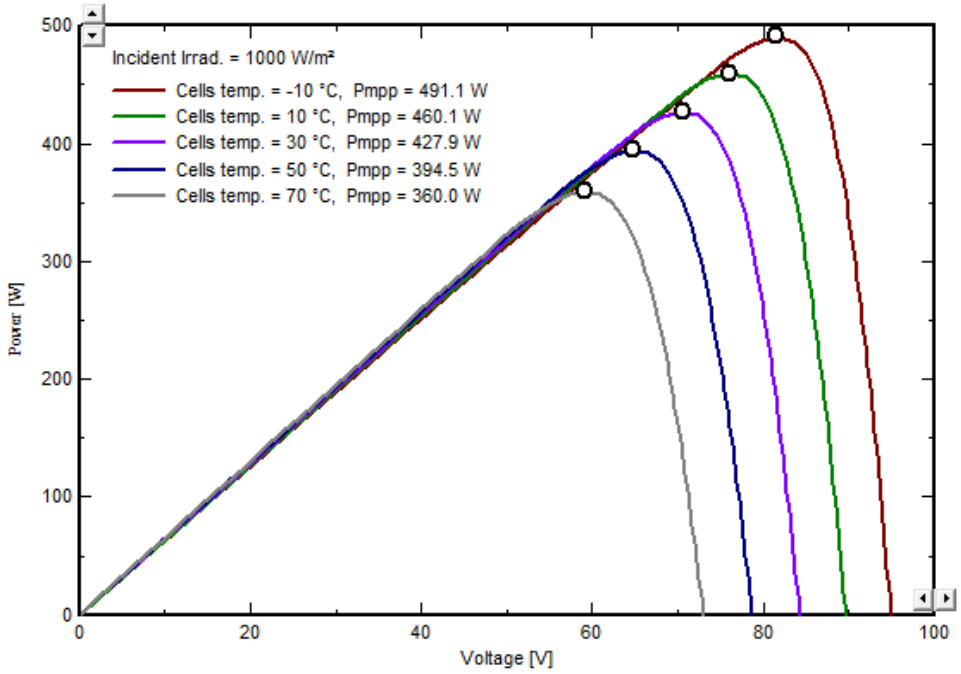

Figure 2.12: The effect of temperature on power output of a PV module, and the maximum power point.

Figure 2.13 illustrates the efficiency as a function of incident global radiation at different temperatures. The figure shows that the efficiency decreases with decreasing irradiation. Under Standard Test Conditions (STC)[7], the efficiency is 20.17 %, but has relative efficiency loss with respect to STC by -0.2 % at 800 W/m^2 up to -3.0 % at 200 W/m^2. This corresponds to an efficiency reduction of 15 % from 1000 W/m^2 to 200 W/m^2 under STC. Further on, the figure shows a significant drop in efficiency as the temperature increases. If the temperature increases with 15 °C from 25 °C, the efficiency decreases by 5 %. For a temperature increase of 35 °C from 25 °C, the efficiency decreases by 13 %. However, if the temperature decreases from STC, the efficiency increases. For a temperature decrease of 15 °C from STC, the efficiency will increase with 5 %. By looking a the figure it is evident that a temperature decrease of 35 °C leads to a 13 % increase in efficiency, reaching an efficiency of 22.8 %.

7. These values are obtained from testing under Standard Test Conditions: Irradiation intensity 1000 W/m^2, spectral distribution AM1.5 and a temperature of 25 °C.

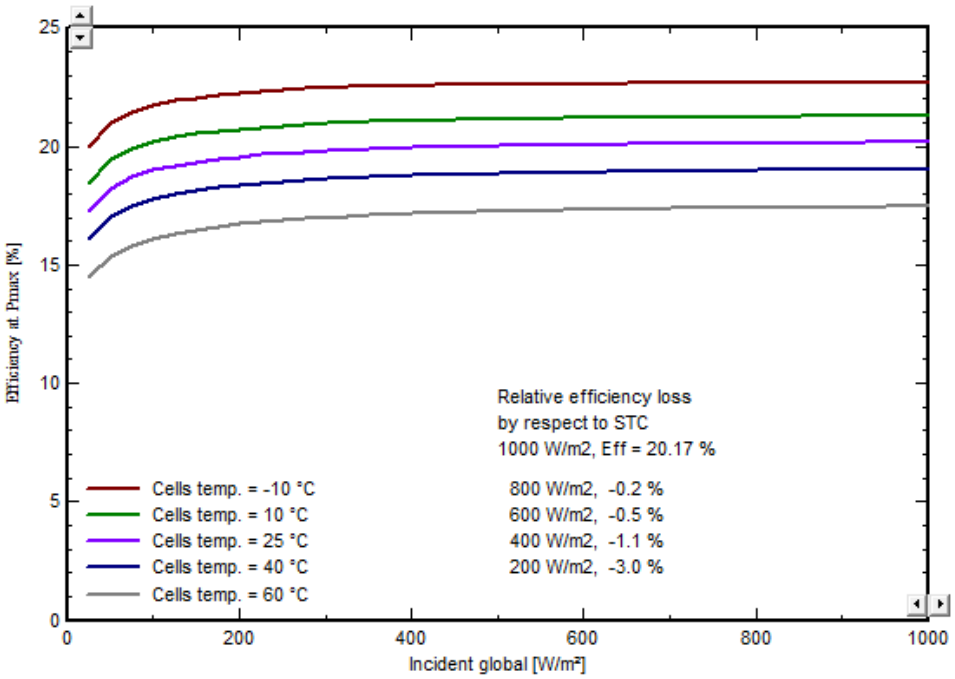

Figure 2.13: Efficiency as a function of incident global radiation at different temperatures.

If one of the cells in series connection in the module is shaded, the current declines [Solanki, 2015]. If the cell is fully shaded it might break down and it could be permanently damaged. It is also important to note that the current output of the series connection is equal to the cell with lowest current output. Hence, a shaded cell will decrease the current output of the module.

Moreover, the PV modules will degrade with time leading to a loss in efficiency. The degradation can be caused by temperature, humidity, type of climate, mismatches, mounting, and so on [Jordan et al., 2016]. For commercial silicon solar cells the average degradation rate is 0.8 %/year.

2.3.7 Mismatch in Cells and Modules

The series and parallel connection of solar cells can lead to mismatches between the cells and the modules due to differences between the cells [Solanki, 2015]. These differences arises due to different processing of the cells, shading, broken glass cover, damage from UV light, same type of cells but from different manufacturer, and so on. The series and parallel connections gives higher power output from the modules and arrays, but if the cells do not have identical

electrical parameters, some of the power is lost. When a mismatch occurs, the best case scenario is loss in output power, and the worst case scenario is physical damage to the modules that might not be repairable. The most common mismatches occur due to mismatch between the open circuit voltage, V_{OC}, and the short circuited current, I_{SC}, in the cells.

2.3.8 Array Design

A PV array consists of both series and parallel connections of PV modules. The number of modules in a string - series connection of modules - depends on the voltage required to turn the inverter on and maximum inverter input voltage. The minimum string length must deliver at least enough voltage equal to minimun inverter voltage, while the maximum string length has to generate less voltage than maximum inverter input voltage [Ahmed et al., 2016]. To calculate the minimum number of modules in a string, the following equations are used.

$$Maximum\ number\ of\ modules\ per\ string = \frac{V_{HI}}{V_{HM}} \tag{2.6}$$

$$V_{HM} = V_{OC} + V_{inc} \tag{2.7}$$

$$V_{inc} = -T_L \cdot Temperature\ coefficient\ of\ V_{oc} \tag{2.8}$$

where V_{HI} is the maximum acceptable inverter voltage, V_{HM} is the highest voltage expected from each module, T_L is the difference of lowest ambient temperature from STC, and V_{OC} is the open-circuit voltage at STC. The following equations are used to calculate the minimum number of modules per string.

$$Minimun\ number\ of\ modules\ per\ string = \frac{V_{LI}}{V_{LM}} \tag{2.9}$$

$$V_{LM} = V_m + V_{dec} \tag{2.10}$$

$$V_{dec} = T_H \cdot Temperature\ coefficient\ of\ V_{OC} \tag{2.11}$$

where V_{LI} is the minimum acceptable inverter voltage, V_{LM} is the lowest voltage expected from each module, T_H is the difference of highest ambient temperature from STC, and V_m is the voltage of the module at maximum power at STC.

2.4 Converters

The PV system relies upon converters to operate as charge controllers, maximum power point trackers and for interfacing different types of load to the PV source [Solanki, 2015]. A converter is a device that converts one DC signal into another DC signal, and can additionally be used for noise isolation or current boosting. The converter will have a maximum power point tracking in order to maximize the power output.

For large marine vessels such as wind farm support vessels, there will be a hybrid system consisting of a fuel oil motor and PV arrays. The two systems will work together to generate enough power required to operate the vessel. Due to recent innovations in power electronics and the fact that PV systems, storage devices and modern electronic loads are inherently DC, the conventional AC grids are now being replaced by DC grids in the on-board integration [Ahmed et al., 2016]. By doing so, it is possible to achieve higher efficiency due to a reduction in number of conversion steps when connecting the power sources to different devices. In addition, DC grids introduces the possibility to have variable speed on engines, which gives higher fuel efficiency at lower loads. The use of DC grids also leads to lower emissions due to a more efficient system, and since there is no AC switchboard, less space is required for installation which leads to weight reduction. However, by using only DC grids, the system becomes more complex. Figure 2.14 illustrates a potential arrangement for the multi-source network. The network consist of PV arrays, a diesel generator, a DC bus, converters, a storage system, and different loads.

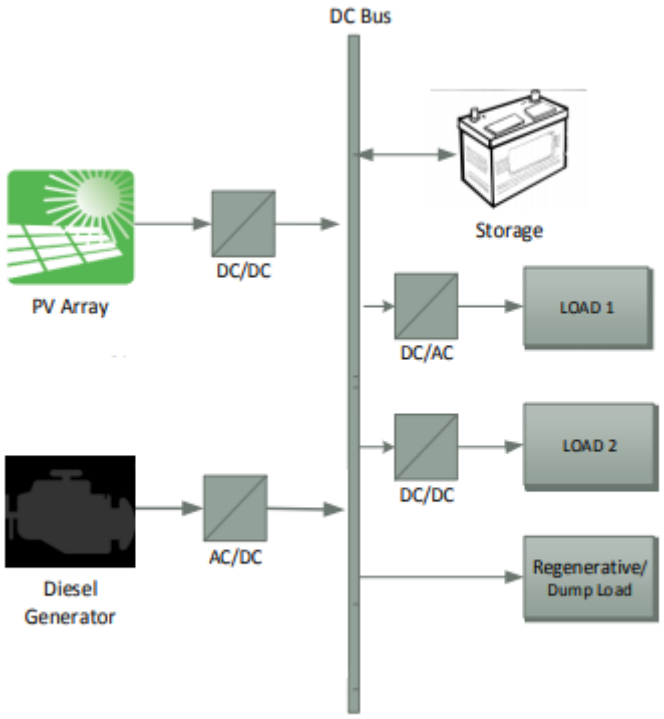

Figure 2.14: Block diagram of potential multi-source renewable energy ship powering network with DC grid, as explained in [Ahmed et al., 2016].

2.5 Batteries

Batteries can be used in PV systems to store energy when the PV modules produces more energy than being consumed, and when the PV modules produces less energy than the consumer needs, the energy stored in the battery can be used. However, the land-based system simulated in this thesis will use the grid as a virtual battery. The reason being that a battery at this site would need to have a capacity of 600 MWh in order to supply the ferry throughout the winter. A battery of this size corresponds to the battery package of 6 000 Tesla Model S 100d [Tesla, 2018]. In addition, a battery of 600 MWh requires a lot of space and would be very expensive. For a PV system installed on a vessel, it is assumed that the generated power will not exceed the consumed power at any time. Therefore, a battery will not be included in the simulations for neither systems.

2.6 Motion of the Ocean

The linear wave theory describes ocean surface waves, and is used in both ocean and coastal engineering and naval architecture [Gudmestad, 2015]. This theory regards waves as sinusoidal shaped waves, and are called regular waves. In real life, the waves are a combination of many waves with different heights and periods that are called irregular waves. These waves can be analysed by Fourier analysis as a sum of regular waves. Waves analysed by Fourier analysis are higher-order waves that have approximately 10 % higher amplitude than regular waves. The waves closest to a sinusoidal shape are swell waves and waves occurring due to wind from the same direction over a long period of time. The sinusoidal waves have a surface profile described by the following equation.

$$\xi = \xi_0(x,t) = \xi_0 sin(\omega t - \kappa x) \tag{2.12}$$

where ξ_0 is the amplitude, ω is the angular frequency of the wave, t is the time, κ is a constant known as the wave number and x is the position. Since the surface profile is described by a sinusoid, and the average of a sinusoid is equal to zero, i.e. surface of the ocean without waves, the vessel will, on average, sail in a horizontal direction. Further on, this can be used when considering a vessel with PV modules on the weather deck. As the vessel move in its six degrees of freedom (heave, surge, sway, yaw, roll and pitch), the angle of the incident radiation on the modules will change. Since the surface profile is a sine function, the vessel will, to some extent, move in a repeating motion and the surface which the modules are mounted on can, on average, be regarded as horizontal.

3

Economic Aspects

This chapter identifies the costs concerning operation and maintenance (O&M) of PV systems, along with carbon and nitrogen oxide taxes, and fuel costs. In addition, the future cost reduction potentials of total installed costs will be discussed, along with reasons for potential cost reduction.

3.1 Operation and Maintenance Costs of PV systems

The share of operation and maintenance cost of PV systems has increased significantly over the last five years due to decrease in installation costs of PV modules [IRENA, 2018]. For grid connected utility-scale systems in the United States, O&M costs reportedly lie between 10-18USD/kW per year. Figure 3.1 illustrates the shares of O&M by category for grid connected utility-scale PV systems in UK. A study in 2014 from the United Kingdom looked into the O&M costs and suggested that maintenance costs accounted for 45% of total O&M costs and land lease for 18%. Moreover, local rates/taxes accounted for 15%, insurance for 7%, site security and administration costs for 4% each, and utilities, including electricity purchase, accounted for 2%.

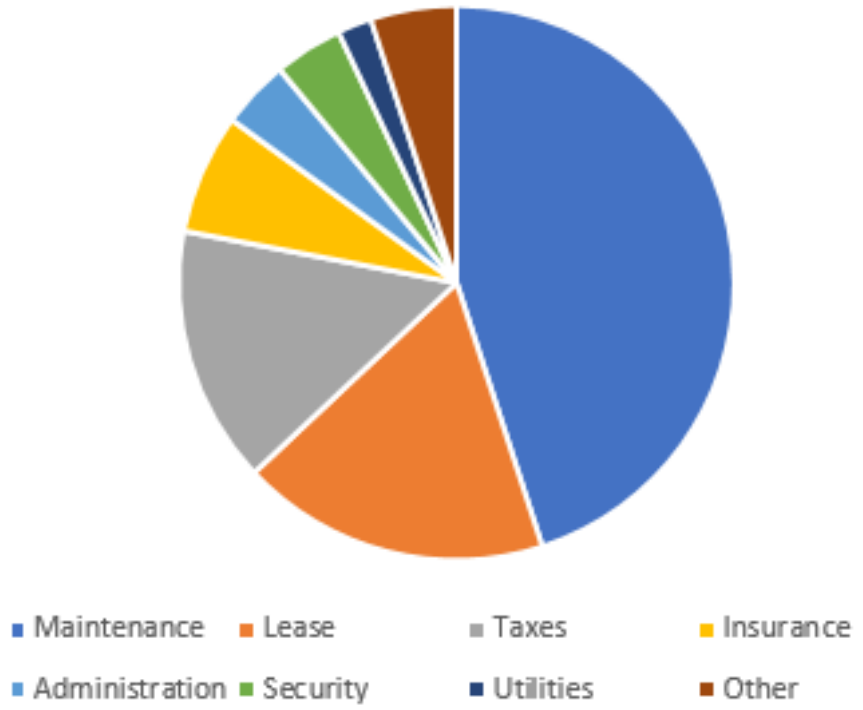

Figure 3.1: Share of operation and maintenance costs for utility-scale systems in UK in 2014 by category [IRENA, 2018]

Figure 3.2 illustrates the total installed costs for utility-scale PV systems for different countries divided into three subcategories; hardware, installation, and soft costs. The figure shows that the module and inverter costs make up about half of total installed costs in the cost competitive countries, while it accounts for about one third in the other countries. The module and inverter costs vary from about 450 USD/kW in India and China to around 700 USD/kW in Japan and the United States. Figure 3.2 also illustrates that the installation costs vary by country, and for the countries represented, the price varies from approximately 100 USD/kW to 400 USD/kW. Balance of system (BoS)[1] costs (excluding inverter) accounts for about half of the total installed costs in countries with competitive installed costs. The soft costs are a part of the BoS costs and accounts for about one third of the BoS costs. Out of the total installed costs, the soft costs make up about 17 %, on average. Based on Figure 3.2, an exchange rate of 7.76 NOK/USD and some reduction in price due to volume discount, one PV module from *SunPower* is estimated to cost 3000 NOK [Norges Bank, 2018].

1. Balance of system includes batteries, battery charge controllers, converters, inverters, racking and mounting, protection relays and other installation and hardware equipment.

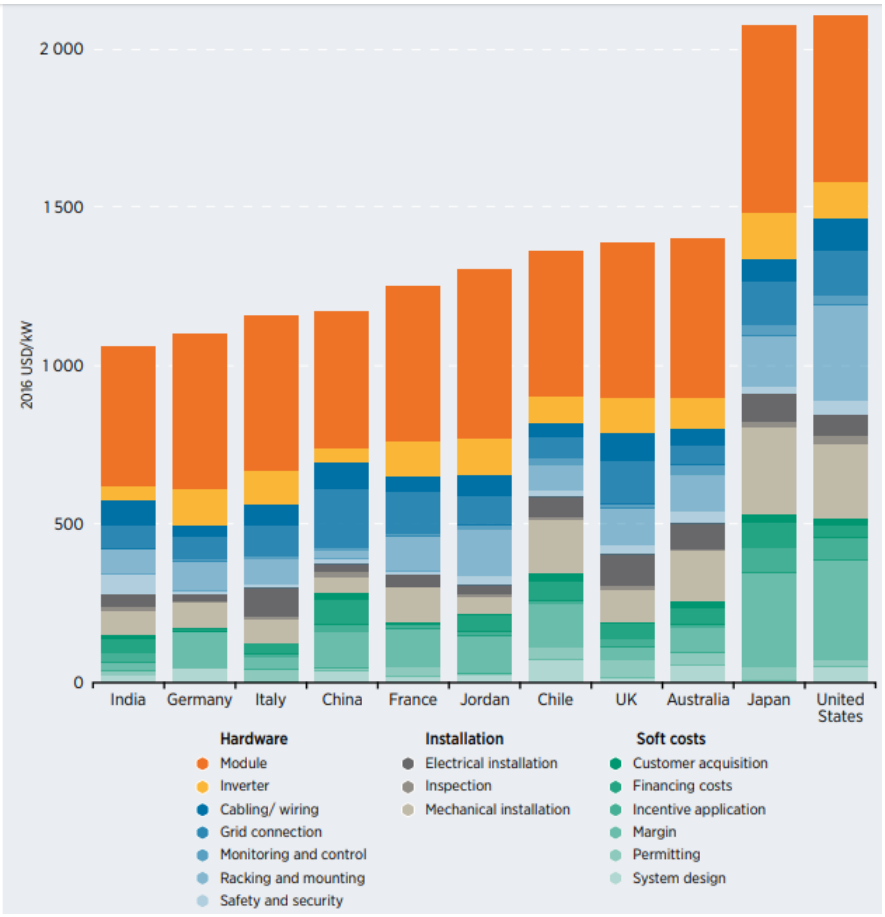

Figure 3.2: Detailed breakdown of utility-scale solar PV total installed costs by country in 2016 [IRENA, 2018]

3.2 Fuel and Tax costs

The Norwegian Tax Administration (NTA) has a tax on emissions of nitrogen oxides (NOx) occuring due to energy generation from the following sources [NTA, 2018]: "Propulsion machinery with a combined installed engine power output of over 750 kW. Engines, boilers and turbines with a combined installed power output of over 10 MW. Flaring on offshore installations and onshore plants" (The Norwegian Tax Administration, NOx tax, 23. Jan. 2018).

The NOx tax applies to emissions from shipping in Norway and on the continental shelf, and will be calculated based on kilogram of actual NOx emissions [NTA, 2018]. As of 2018, the cost of each kilogram NOx is 21.94 NOK/kg. However, there are some exemptions to the tax; vessels used for direct international

shipping, and ships sailing in remote waters for fishing and hunting. In addition, the business organisations that have signed the Environmental Agreement on NOx 2011 – 2017 are exempted.

The global average bunker price (GABP) for marine gas oil (MGO) is 691.50 USD/mt per 28. Mar. 2018 according to *Ship & Bunker* [Ship & Bunker, 2018]. Where the trend in GABP is a linear regression of GABP for LNG-MGO equivalents for a specified time period, which shows the overall direction of the market. The global average LNG price is approximately 7.2 USD/MMBtu per 1. of April 2018 [Bluegold Research, 2018]. In order to get the price in USD/mt a conversion ratio of 52.64 MMBtu/mt will be used [S&P Global Platts, 2017]. Thus, the global average price of LNG will be 379 USD/mt.

The International Maritime Organizations Tier III NOx regulation applies to marine diesel engines of more than 130 kW power output, but if they are used for emergency purposes only, the vessel is exempted from this regulation regardless of the vessels tonnage [IMO, 2018]. Vessels constructed on or after the 1. of January 2016 with installed marine diesel engines and operating in North American and United States Caribbean Sea Emission Control Areas should fulfil the Tier III NOx standards. For vessels operating outside the Emission Control Areas, the Tier II regulation applies. Table 3.1 shows the NOx regulations for ships after a certain construction date, and the emission limit for engines with different rpm.

Table 3.1: Tier I, II and III NOx emission regulations for engines operating at different rpm's [IMO, 2018].

Tier	**Ship construction date after**	**Total weighted cycle emission limit (g/kWh) n = engine's rated speed (rpm)**		
		$n < 130$	$n = 130\text{-}1999$	$n \geq 2000$
I	1 January 2000	17.0	$45 \cdot n^{(-0.2)}$	9.8
II	1 January 2011	14.4	$44 \cdot n^{(-0.23)}$	7.7
III	1 January 2016	3.4	$9 \cdot n^{(-0.2)}$	2.0

The following two engines are the ones used in the vessels to be discussed. For calculation purposes, both engines have generalized fuel consumption and emissions of CO_2 and NOx. Rolls-Royce's Bergen C25:33L engine has a specific fuel consumption of approximately 185 g/kWh of liquid fuel, and it varies with revolutions per minute and load [Rolls-Royce plc, 2017a]. However, a specific fuel consumption of 200 g/kWh is generally used for calculations. This engine is estimated to emit 610 gCO_2/kWh, based on values from Rolls-Royce.

The Bergen C26:33L is one of Rolls-Royce's gas engines, and has a specific energy consumption of 7550 kJ/kWh [Rolls-Royce plc, 2017a]. However, the specific energy consumption is taken to be 8305 kJ/kWh for calculations. According to numbers from Rolls-Royce, this engine is estimated to emit 450 gCO_2/kWh.

Table 3.1 will be used to calculate the Tier II and Tier III NOx emissions for an engine operating at 750 rpm, which will be the operating speed of the engine, according to Rolls-Royce.

$$\text{Tier II NOx emission:} \quad 44 \cdot 750^{-0.23} \approx 9.6\,\text{g/kWh} \tag{3.1}$$

$$\text{Tier III NOx emission:} \quad 9 \cdot 750^{-0.2} \approx 2.4\,\text{g/kWh} \tag{3.2}$$

The numbers achieved in equation 3.1 and 3.2 can now be used to calculate the cost of marine gas oil and NOx tax per kWh produced. The exchange rate for USD will be taken as an average of daily prices during March 2018 and is 7.76 NOK/USD [Norges Bank, 2018]. In the government budget by the Ministry of Finance, the proposed general and continental shelf tax for CO_2 emissions from light oil (MGO) for 2018 is 458 NOK/mtCO_2 and 398 NOK/mtCO_2, respectively [Finansdepartementet, 2018]. For CO_2 emissions from liquified natural gas for domestic routes in Norway and on the continental shelf, the proposed tax is 457 NOK/mtCO_2 and 453 NOK/mtCO_2, respectively. Further calculations will be executed with the domestic taxes since both vessels are assumed to operate in domestic waters, and the fact that the domestic tax is higher than continental shelf tax.

Table 3.2 shows fuel costs for the Bergen C25:33L and the Bergen C26:33L engines running on MGO and LNG, respectively. In addition, the table presents domestic emission taxes for NOx and CO_2 emissions, and the combined fuel and emission tax cost. The NOx tax is greater for engines operating under Tier II regulations than engines operating under Tier III regulations due to an increased amount of allowed NOx emissions per kWh, as calculated in Equation 3.1 and Equation 3.2. By looking at the table it is evident that the domestic CO_2 emissions from burning MGO costs more than CO_2 emissions from burning LNG. For the fuel and emission tax cost, the fuel cost and domestic emission tax for both CO_2 and NOx were added together and multiplied by 1.4. The multiplication factor 1.4 arises due to value added tax and different operation costs. From the table it is clear that the fuel and emission tax cost for MGO is almost twice as high as the LNG cost for both Tier II and Tier III regulations. The calculations for Table 3.2 are shown in Listing C.1 and Listing C.2 in Appendix C.

Table 3.2: Fuel costs for MGO and LNG and emission taxes for NOx and CO_2 for Tier II and III regulations.

Regulation	Fuel type	Fuel costs [NOK/kWh]	Emission type	Domestic emission tax [NOK/kWh]	Fuel and emission tax cost [NOK/kWh]
Tier II	MGO	1.074	NOx	0.210	2.19
			CO_2	0.280	
	LNG	0.464	NOx	0.210	1.23
			CO_2	0.206	
Tier III	MGO	1.074	NOx	0.053	1.97
			CO_2	0.280	
	LNG	0.464	NOx	0.053	1.01
			CO_2	0.206	

3.3 Cost Reduction Potential of Solar PV

This section focuses on the future cost reduction potential for PV systems along with reasons for the potential cost reduction. The cost reduction potentials for modules, inverters and BoS systems will be analysed separately, before combining them and estimating the total cost reduction potential in 2025. These estimates are based on costs in 2015, and the analyses are based on a scenario driven by three factors. [2]

3.3.1 Total System Costs

According to *IRENA's REmap: Roadmap for a Renewable Energy Future* the rapid growth in solar PV will continue, and total installed capacity will lie between 1750 GW and 2500 GW by 2030 [IRENA, 2016a]. The report suggests that the global average total installed costs of utility-scale PV systems could experience a 53 % reduction in 10 years, falling from around 1.8 W/USD in 2015 to 0.8 W/USD in 2025. If the uncertainty around cost drivers are taken into account, the costs could decrease by anywhere between 43-65%.

Figure 3.3 illustrates the past and potential future global weighted average (GWA) total system costs breakdown of utility-scale solar PV systems from 2009 to 2025 [IRENA, 2016b]. From 2009 to 2015 the BoS costs (excluding inverter) increased from 37 % to 60 % of the total installed costs, while the

2. "IRENA has examined the possible impact of technology and market drivers in terms of reducing today's best practice BoS cost. In addition, it has been assumed that countries within the same cost group will converge towards the current bestin-class level for that cost group over the next decade. Finally, it is assumed that only new and emerging markets will remain in the high-cost group by 2025, while others shift from high cost to medium cost and from medium cost to low cost structures." (IRENA, 2016, pp.38).

decrease in module prices contributed to a 68 % reduction in total installed costs in the same period.

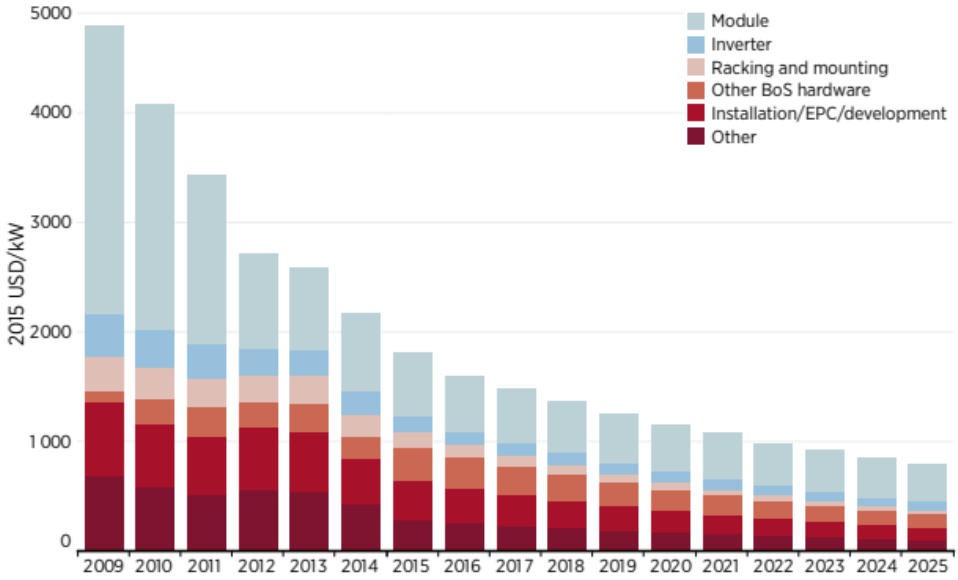

Figure 3.3: GWA total system costs breakdown of utility-scale solar PV systems from 2009-2025 [IRENA, 2016b].

3.3.2 Balance of System Costs

As increasing competitive pressure in the market leads to a convergence towards best practice cost structures, the balance of system costs for utility-scale PV systems could drop by 55-74 % between 2015 and 2025 [IRENA, 2016b]. Figure 3.4 shows the past and potential future BoS costs by source for GWA utility-scale PV systems. By looking at Figure 3.4 one can see that one-third of the potential cost reductions will come from both BoS hardware and soft cost reductions. In 2025, the balance of system costs are expected to be between 0.3 USD/W and 0.5 USD/W, according to estimates made by *IRENA*. It is estimated that convergence towards best practice costs will account for 90 % of the potential cost reductions of the balance of system. The remaining cost reductions occur due to increased efficiency of the modules which will lead to a reduction in area, materials, and labour, and thus lead to a cost reduction of racking, mounting, and installation.

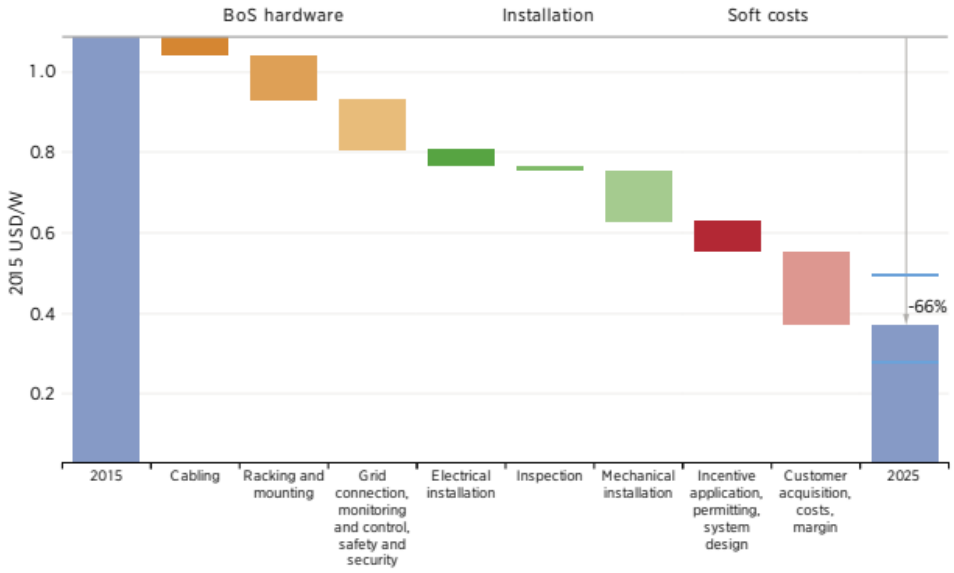

Figure 3.4: The GWA utility-scale PV systems BoS costs in 2015 and potential costs reductions by 2025 by source [IRENA, 2016b].

3.4 Incentives

Enova SF was established in 2001 and is owned by the Ministry of Climate and Environment [Enova, 2018b]. It is an organisation whose goal is to change the way the population uses energy and accelerate the change toward renewable energy. Enova gives incentives to companies investing in technologies that reduce green house gas emissions [Enova, 2018a]. In the marine sector these technologies could be propulsion systems, engines, ventilation and so on. The incentives are mainly given to vessels that operate in the Norwegian economic zone and/or vessels that regularly arrives Norwegian ports. Companies that apply for the incentives apply for the amount needed to get a positive investment decision, and can get up to 30 % of the additional expenses.

4

Vessels and Geographical Area

The vessels considered in this thesis will be wind farm support vessels with PV modules as supplementary power source. In addition, fully electric ferries operating in-land in Norway with power generated from a land based power station will be considered. The vessels and locations used in this thesis are only used as examples.

4.1 Edda Passat

Edda Passat is a wind farm support vessel operated by *Østensjø* shipping company, and was built by *Gordan* in 2017 [Østensjø Rederi, 2018]. The ship is designed by Rolls-Royce Marine with the UT540WP design and is illustrated in Figure 4.1. In addition, Rolls-Royce Marine delivers the complete power, propulsion, and automation system, and is responsible for the engineering. The products delivered includes electrical system, engines, bridge controls, dynamic positioning system, and so forth. Edda Passat will be used as a wind farm support vessel in the Hornsea Zone. Edda Passat consumes an estimated 4.27 mt/day, which corresponds to 128 mt/month, and an energy usage of 8 538 kWh/day, corresponding to 256 MWh/month. The calculations are shown in Listing C.3 in Appendix C.

Figure 4.1: Aerial view of the wind farm support vessel Edda Passat [Østensjø Rederi, 2018].

The area of weather deck of the ship can be estimated by multiplying the ships length over all (LOA) with the breadth (B) of the ship and the actual area in relation to its circumscribed rectangular, this ratio will be referred to as N [Transocean Coatings, 2018]. Edda Passat have a length of 82 m and a breadth of 17 m, and will be considered to have the same N as a cargo vessel, N = 0.88 [Østensjø Rederi, 2018]. Thus, the area of the weather deck of Edda Passat is:

$$\begin{aligned} A_{\text{EP}} &= LOA \cdot B \cdot N \\ &= 82\,\text{m} \cdot 17\,\text{m} \cdot 0.88 \\ &\approx 1227\,\text{m}^2 \end{aligned} \tag{4.1}$$

From Figure 4.1 it is evident that there are some inclined surfaces, marked by purple lines, above and below the navigation bridge and on the front tip, green area, that could be suitable for installation of fixed PV modules. In addition, the horizontal surfaces, blue area, on the front deck could be suitable for installation of fixed/flexible PV modules depending on what these areas are used for. If, for example, the horizontal surfaces needs to walkable, flexible PV modules could be installed as they can be walked upon. Taking the inclined surfaces into consideration, an estimated area of 184 m^2, equal to 15 % of the weather deck, could be used for installation of PV modules. The horizontal area that could be used for installation of PV modules is estimated to 246 m^2, equal

to 20 % of the weather deck. If both the horizontal and inclined surfaces are taken into consideration, an estimated 430 m^2, equal to 35 % of the weather deck, could be used for installation of PV modules. Further on, a row of PV modules could be installed on the top of the hull, marked by black lines, where an estimated area of 78 m^2, 39 m^2 on each side, could be used for installation of PV modules. The available area on the rear deck is not suitable for installation of PV modules due to the ship's function. The total available installation area on Edda Passat is estimated to be 508 m^2.

Figure 4.2: Sketch of possible installation areas on Edda Passat. Black area corresponds to $\beta = 80°$, blue represents horizontal surface, green area corresponds to $\beta = 15°$and purple represents area with $\beta = 35°$.

4.2 Hornsea Wind Farm

For this thesis, a wind farm support vessel operating at the Hornsea wind farm right outside of England will be used. The Hornsea wind farm project is owned by *Ørsted*, formerly *DONG Energy*, and is divided into three projects [Ørsted, 2015]; Hornsea Project One and Two which are under construction, and Hornsea Project Three which is under development [Ørsted, 2018]. The Hornsea Zone stretches across 4 000 km^2 and is located between 31 and 190 km off the coast of Yorkshire, as illustrated in Figure 4.3 [Ørsted, 2015], and

Project One's geographical centre lies at a latitude of 54.883° and a longitude of 1.922° [4C Offshore Ltd, 2018]. Project One will have a capacity of 1.2 GW and will be the largest offshore wind farm in the world, according to Ørsted. Project Two and Three are estimated to have a combined capacity of 3 GW.

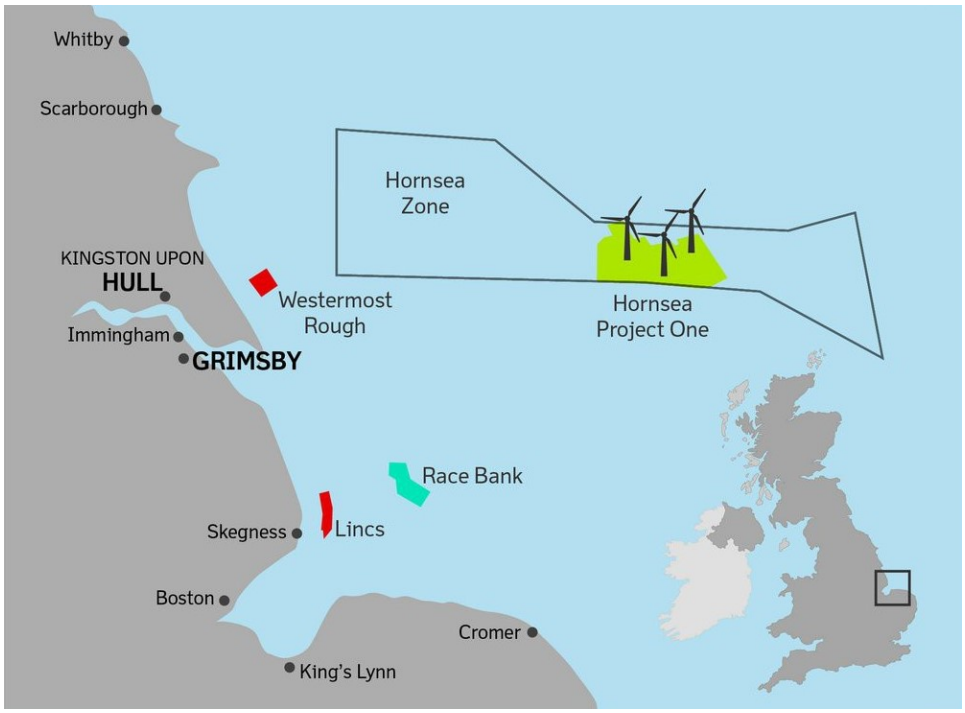

Figure 4.3: Map of Hornsea wind farm project area [offshoreWIND, 2017]

4.3 MF Ampere

The car and passenger ferry MF Ampere was the first fully electric ferry of its kind, and its propulsion system is two azipull azimuthing thursters delivered by Rolls-Royce [Stensvold, 2015]. It operates in Sognefjorden between Lavik and Oppedal, and uses 20 minutes on the passage. The zero emission ferry is built by *Fjellstrand* and is owned by *Norled*. MF Ampere has two battery packages installed with a capacity of 500 kWh each, and the ferry consumes approximately 150 kWh per passage [Stuards, 2015]. The ferry makes 34 crossings each day, which corresponds to an energy consumption of 5.100 kWh/day, and an energy consumption of 1836 MWh/year.

The weather deck of MF Ampere will be calculated in the same way as for Edda Passat, but with a $N = 0.91$, breadth of 20.8 m, and a length of 80.8 m [Stensvold, 2015]. Hence, the area of the weather deck of MF Ampere is:

$$\begin{aligned} A_{\mathrm{A}} &= 80.8\,\mathrm{m} \cdot 20.8\,\mathrm{m} \cdot 0.91 \\ &\approx 1530\,\mathrm{m}^2 \end{aligned} \tag{4.2}$$

Figure 4.4: Aerial view of the fully electric car and passenger ferry MF Ampere [Stuards, 2015].

From Figure 4.4 it becomes clear that there is no available space for installation of PV modules with this design. If PV modules were installed on the deck, it would be shaded almost all the time due to cars standing on top of it. But, if a framework were installed above the deck, there would be a lot of available space for installation of PV modules. The available are could come close to 80 % of the weather deck, equal to around 1224 m^2. But, this scenario is very unlikely and due to the high mountains surrounding this fjord, a PV power station near Lavik would be a better option. However, for ferries operating in a more open area, a framework with PV modules could be installed as a supplementary power source.

4.4 Lavik-Oppedal

The distance Lavik-Oppedal is a part of the road E39 and stretches across Sognefjorden, as illustrated in Figure 4.5. At each ferry landing there is a boost battery charger with a capacity of 300 kWh [Stensvold, 2015].

(a) **(b)**

Figure 4.5: a) Outline of the location of the passage, and b) the passage from Lavik to Oppedal [Kystverket, 2018].

In Figure 4.5b there is a blue dot about 2 km outside of Lavik which represents the potential location of a PV power station. It is located at a latitude of 61.1° and a longitude of 5.54°. This location was chosen due to an almost flat surface on both sides of the road, as illustrated in Figure 4.6, and its closeness to the ferry landing. In addition, PV modules installed on the location can be oriented due south, which is the optimal orientation, as discussed in Subsection 2.3.4, and horizon shadings are very low. The surface condition leads to less construction costs for making the site suitable for installation of a PV power station. In addition, this site is close to the road and the grid, as seen in Figure 4.6, where the black line in the top left corner represents the grid. Thus, there will be small costs concerning infrastructure. The shaded area in Figure 4.6 equals 61 500 m^2, which corresponds to approximately 12 standard sized football fields.

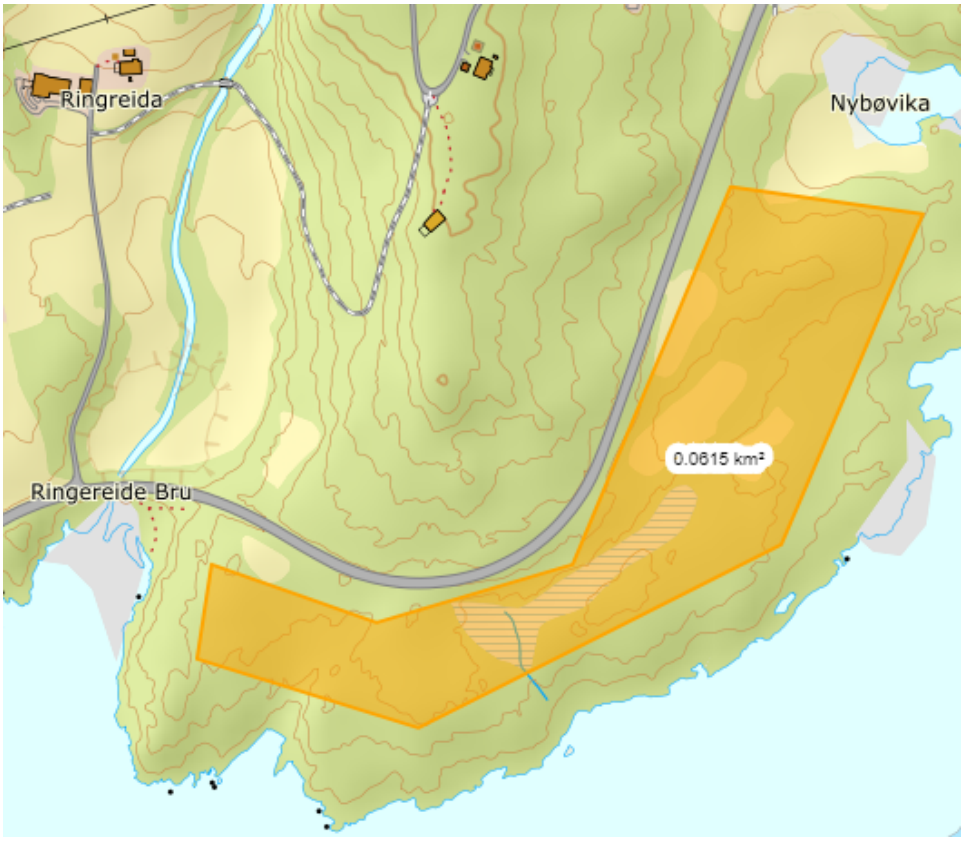

Figure 4.6: Potential installation area [Kystverket, 2018]

Another option is to install a PV power station on the sea just by the ferry landing. The advantage of installing such a system at sea rather than on land is that the water can be utilized to cool down the system, leading to increased power production. Further on, it can be very expensive to buy land, depending on who owns it and if there are any plans for the area, thus, renting an area on sea is probably cheaper. However, the disadvantages is that there are too rough sea conditions for such a system to be installed at this location, and the modules needs to withstand corrosion due to salt water.

5

Simulation Software and PV Modules

The chapter examines the simulation software used to simulate the PV system connected to the grid. In addition, it presents the PV module used for simulations and its key characteristics. In addition, it takes a brief view at the potential future evolution of solar PV for marine applications.

5.1 PVsyst

PVsyst Software is a simulation software designed to be used on PV systems, and is developed by *PVsyst SA* [PVsyst, 2014]. The software is designed for use on grid-connected, stand-alone, pumping, and DC-grid PV systems. The software has a database of meteorological data and PV systems components that can be used for simulations.

The meteorological data can either be retrieved using *Meteonorm*, NASA-SSE (Surface Meteorology and Solar Energy programme), or imported data retrieved from other sources [PVsyst, 2014]. Since solar radiation data can be imported from many different meteorological databases, any location on the planet can be created in *PVsyst*. Anyhow, *Meteonorm* will be used as a meteorological database for this thesis. The monthly average radiation values were

calculated based on data from ground stations, and for a period of at least 10 years. In remote areas, satellite data is used for radiation interpolation. For sites located more than 50 km away from a station, satellite data is used. If the nearest ground station is more than 30 km away from the site, a combination of data from the ground station and satellites will be used. Hourly values are generated synthetically by using stochastic models, and it is therefore a uncertainty concerning these values.

By using the *Project Design* model of *PVsyst* a very detailed system design with hourly values can be simulated [PVsyst, 2014]. The system can consist of PV arrays connected to the grid, where the software assists in choosing the size of the PV array and the right inverter. It is also possible to define more detailed parameters such as thermal behaviour, shading, incidence angle loss, and so on. In total, there are 50 different parameters that needs to be defined before simulating the system.

The results obtained from the simulation are summarized in a report, which comprises of all parameters used during the simulation and a short description of the main results [PVsyst, 2014]. All the variables used in the simulation are stored in monthly values, and can be viewed in graphs at any time. In addition, the software stores hourly values for some pre-chosen variables. For even more detailed information, graphs of energy loss diagram, normalized yield, performance ratio, incident energy, and so on can be viewed as monthly or daily values. To find the cost benefits of such a system, an economic evaluation, based on the defined parameters and simulation results, can be run after the simulation.

PVsyst has many predefined physical parameters and models in order to run the systems defined by the user [PVsyst, 2014]. These predefined values are reasonable values which were defined by the author and can be used in most scenarios. However, these values can be changed depending on the situation or hypothesis. The parameters can be found in categories like grid-connected system, system design parameters, detailed simulation verification conditions, PV modules, and so on. As far as changing the code in *PVsyst* goes, the latter parameters mentioned are the most one can change it.

5.2 Simulation Scenarios

The PV system aboard Edda Passat will be designed as grid connected due to the fact that produced energy will not exceed consumption at any times. Since this system will be installed on available surfaces on the weather deck, the tilt angles are predefined. In addition, the ships orientation is likely to change often, and the system will therefore be simulated with different orientations. The system will be simulated with orientations north, east, south and west with four different tilt angles: 0°, 15°, 35° and 80°.

The project design for a PV power station near Lavik will be a grid connected system, which will focus on producing as much energy as possible during the year, and will therefore have a tilt angle that optimizes yearly production. This power station will be designed to produce enough energy throughout the year to cover the yearly consumed energy by MF Ampere. Since it is grid connected the energy produced will be transferred directly to the grid. The boost battery charger at the ferry landing in Lavik is also connected to the grid and will at all times use whatever is necessary to charge the ferry.

In practice, the power station will produce more energy than consumed by MF Ampere during the summer, but during winter, the power station will not be able to produce enough energy to operate MF Ampere. The needed energy will be imported from the grid, and excess energy will be sold to the power company. For regions with an unstable and weak grid, such as Lavik, a PV system can help stabilize the grid. The utility-scale PV system can help stabilize the regional grid through new inverter technology. This technology can act as phase shift oscillators, helping the phases of power production and transmission in sync [Fairley, 2015]. The energy produced by a PV power station in Norway will compete with energy from hydro power stations, and thus replaces renewable energy with renewable energy. However, the more renewable energy produced in Norway, the more can be sold to Europe, where renewable energy can replace power from coal power plants and gas-fired power stations.

For both simulations there are some parameters that affects the produced power more than others. The most important parameters are the tilt angle and the azimuth angle. If there is no horizon shading nor near shading, the optimal azimuth for a system located on the northern hemisphere is zero degrees, i.e. oriented due south, and vice versa for a system located on the southern hemisphere [Solanki, 2015]. However, horizon and near shading can lead to an optimal azimuth angle other than due south. The tilt angle will vary depending on the latitude of the location, but *PVsyst* calculates the optimal tilt angle for any location. Horizon and near shading will also affect power production from the system, where power production decreases with increasing shading. The horizon shading profile will be defined by using the

European Commission's Photovoltaic Geographical Information System tool [European Commission, 2017].

The albedo radiation is a fraction of the global incident radiation. Its contribution is calculated based on the type of surface in front of the PV modules and depends on the tilt angle of the modules [PVsyst, 2014]. Further on, the array incidence loss occurs because reflection increases with an increasing incidence angle, and corresponds to the decrease of the irradiance actually reaching the surface of the PV cell, with respect to irradiance under normal incidence [PVsyst, 2014]. This parameter is predefined by *PVsyst* depending on the type of PV module, and will not be altered before simulating.

There is also a parameter named soiling loss which calculates power production losses due to snow, leaves, and etc., which decrease the power output from the land-based power station. Another important parameter is the thermal coefficient which varies depending on whether or not the system is free-standing, semi-integrated, or fully integrated. A free-standing system is not mounted on a building or any surface and thus experience more cooling due to wind. The semi-integrated system is installed on a building or similar structures but has a gap between the back of the modules and the structure for ventilation. A fully integrated system is isolated and has no very little ventilation. Hence, a free-standing system will have a higher thermal coefficient and a higher power output than a semi-integrated or fully integrated system.

5.3 Suppliers of PV Modules

There are multiple companies to choose between when ordering PV modules approved for marine environments, and several PV modules from different manufacturers around the world were evaluated. Finally, a PV module from *SunPower* was chosen to be the most suitable for installation in marine environments, and will be used for simulations. The PV modules are tested under STC, hence, all the values given in the table are measured under STC. The framed modules need some sort of fixing brackets in order to be installed on a surface.

5.3.1 SunPower

The E20-435-COM PV module, comprising of monofacial monocrystalline cells, are made by *SunPower*, which is a company based in Silicon Valley in the U.S. that develops high quality solar modules [SunPower, 2018]. Table 5.1 shows some general and electrical data of the E20-435-COM PV module, a more detailed table can be found in Table B.1 in Appendix B [SunPower, 2016].

Table 5.1: General and electrical data for the E20-435-COM PV module [SunPower, 2016].

E20-435-COM	
Parameters	Values
L/W/H	2067 mm / 1046 mm / 46 mm
Module area	2.162 m^2
Weight	25.4 kg
Maximum system voltage	1000 V
Nominal power P_N	435 W_P
Module efficiency	20.17 %
Power output per installed area	201.2 W/m^2
Area per kW	4.97 m^2/kW
Weight per kW	58.39 kg/kW

The solar module has the IEC 61701 standard, and is resistant to large hailstone [SunPower, 2016]. It has a power warranty that guarantees a power production of at least 95 % of given nominal power for the first five years. After five years, the guaranteed power production decreases with 0.4 %/year to year 25. In addition, the PV module has a product warranty of 25 years. These PV modules are not sold separately, which makes it hard to find the price of one module. However, the price per module were estimated to be 3000 NOK in Section 3.1.

5.4 Potential Evolution of PV Modules in Marine Applications

For the advancement of PV technology in marine applications it might be logical to take a look at PV technology used for extraterrestrial applications due to the harsh conditions the technology must endure, long lifetime, and high efficiency. The PV modules used on the International Space Station are developed by NASA Glenn Research Center in Cleveland in conjunction with other tech and university communities, according to Jeremiah McNatt, electrical engineer working in the Power Division at NASA Glenn [Bushong, 2016]. Solar cells for extraterrestrial applications are usually made out of silicon cells covered by thin glass, to avoid degradation, or multi-junction cells made of gallium arsenide and other materials which resist degradation better than silicon cells. The gallium arsenide cells have a better efficiency than the silicon cells, where multi-junction cells have an efficiency of 34 %. Even though these are good cells which can endure harsh conditions, the price is very high due to low volume

production. Thus, a solar cell can cost NASA hundreds of dollars compared to a couple dollars for commercial terrestrial cells. As volume is the biggest driver for cost reductions, these cells could get much cheaper if produced for terrestrial applications in big volumes. But with NASA being one of the developers of these cells, the focus on developing these cells will probably continue to be for extraterrestrial applications rather than terrestrial applications.

Fraunhofer Institute for Solar Energy Systems' Photovoltaics Report include efficiencies of laboratory solar cells, where multi-junction concentrator solar cells have achieved an efficiency of 46 % and monocrystalline silicon cells with an efficiency of 27 % in 2017 [Fraunhofer ISE, 2017]. The *International Technology Roadmap for Photovoltaic Results* 2017 has estimated the expected stabilized efficiencies for commercial double-sided contact and rear-contact cells with different wafer materials, as illustrated in Figure 5.1 [ITRPV, 2018]. From the figure it is evident that n-type back contact mono-Si cells are expected to reach an efficiency of 25.5 % by year 2028.

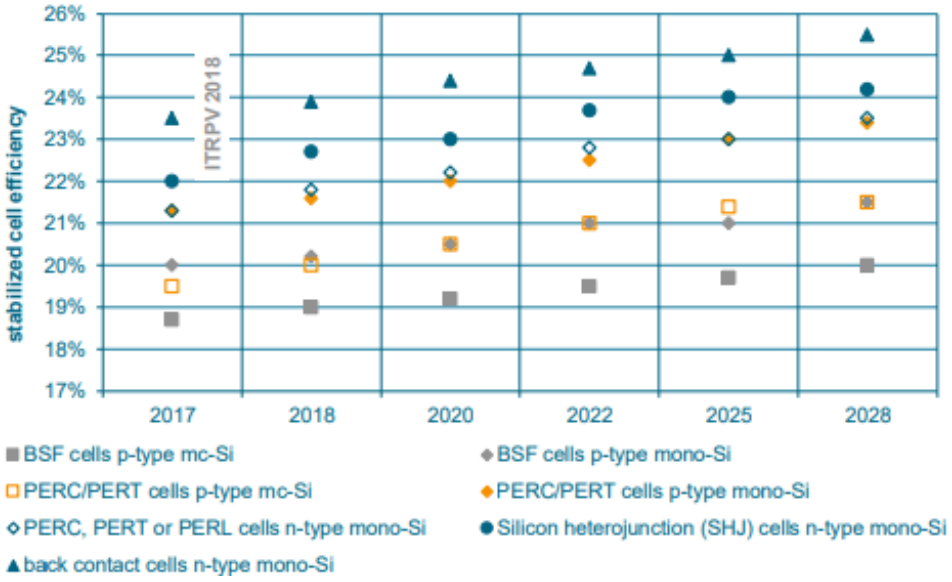

Figure 5.1: Future potential efficiencies for Si-cells [ITRPV, 2018].

6

Results and Discussion

This chapter presents the results obtained from simulations in *PVsyst* for the system at Lavik and the system on Edda Passat. The produced energy, energy cost, and energy distribution will be emphasized. The discussion will focus on production loss due to shading, temperature, and incidence angle. Further on, the energy cost, CO_2 emissions, energy payback time, and break-even point will be discussed. The figures in this chapter were made in *PVsyst* and Excel by using data from simulation reports.

6.1 Power Station at Lavik

The power station at Lavik needs to produce at least 1 836 MWh/year to cover the annual consumption of MF Ampere, and was designed to produce 2 055 MWh/year, with an additional 11 % as a reserve. Such a system covers an area of 16 000 m^2 with a total nominal power of 3 219 kWp, as shown in Table 6.1. From the simulation report in Appendix D, it is evident that the system has a specific energy production of 638 kWh/kWp/year, which indicates the amount of kWh output per installed kWp per year. The average annual energy production per square meter of the system is 132 kWh/m^2/year. The investment cost lies around 31.6 million NOK, annuities at 2.2 million NOK per year and operation and maintenance cost lies around 322 thousand NOK per year, as shown in Table 6.1. Where annuities represents the annual cost in order to pay back the loan over 25 years, corresponding to the guarantee of

the PV modules. In addition, it shows an energy cost of 1.25 NOK/kWh, which is calculated by adding annuities and operation costs and dividing them by yearly produced energy.

Table 6.1: Main simulation results from the power station situated at Lavik

Main simulation results	
Total annual energy production	2 055 MWh/year
Total nominal power	3 219 kWp
Specific energy production	638 kWh/kWp/year
Average annual energy production	132 kWh/m^2/year
Investment	31 567 960 NOK
Annuities	2 239 824 NOK/year
Operation cost	321 900 NOK/year
Energy cost	1.25 NOK/kWh

Figure 6.1 illustrates the effective energy produced by the PV array for each month of the year. The given values for energy production per square meter for each month is taken as the average energy production per square meter per day during that month. Further on, Figure 6.1 shows that the energy production from the array varies throughout the year, with lowest production in December at 0.2 kWh/m^2 and highest production in May at 23 kWh/m^2.

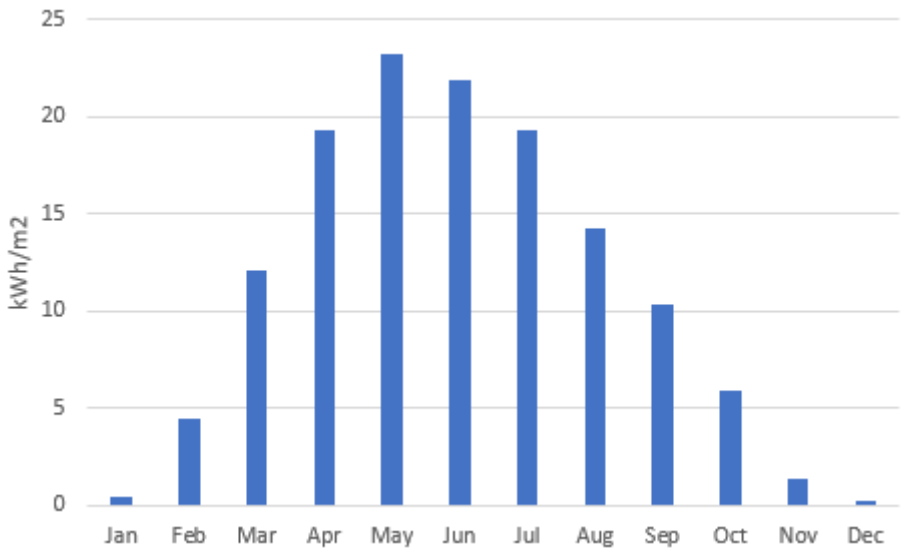

Figure 6.1: Effective energy produced by the PV array located at Lavik for every month throughout the year.

Figure 6.2 illustrates the energy transmitted to the grid for each month of the year. The energy transmitted to the grid varies throughout the year, with the lowest value in December at 2.2 MWh and highest value in May at 362 MWh.

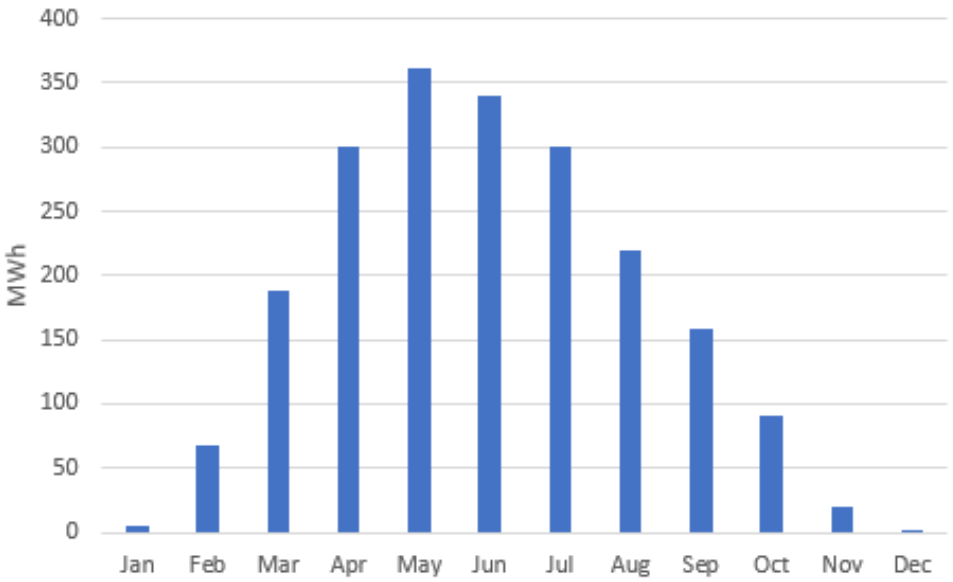

Figure 6.2: Energy transmitted to the grid from the PV array located at Lavik for each month of the year.

Figure 6.3 illustrates the ambient temperature on-site, global incident irradiation in collector plane, and effective global irradiation corrected for array incidence loss and shadings. The figure shows the average ambient temperature for each month over the year, which peaks in July at 16.1 °C and is lowest in February at 1.6 °C. It also illustrates global incident irradiation, which peaks in May at 130 kWh/m^2, and has lowest values in December at 1.4 kWh/m^2. In addition, it shows global effective irradiation throughout the year, which is highest in May at 122 kWh/m^2, and lowest in December at 0.9 kWh/m^2.

Figure 6.4 illustrates hours of sunlight throughout the year, yellow area, and the height of the sun at different azimuth angles. In addition, the figure shows the horizon profile at the power station site, the shaded grey line. The area between the blue lines on each side of the figure illustrates the amount of hours the sun shines on the module. From the figure, it is evident that the most hours of sun occur on June 22, and the fewest hours of sun occur on December 22.

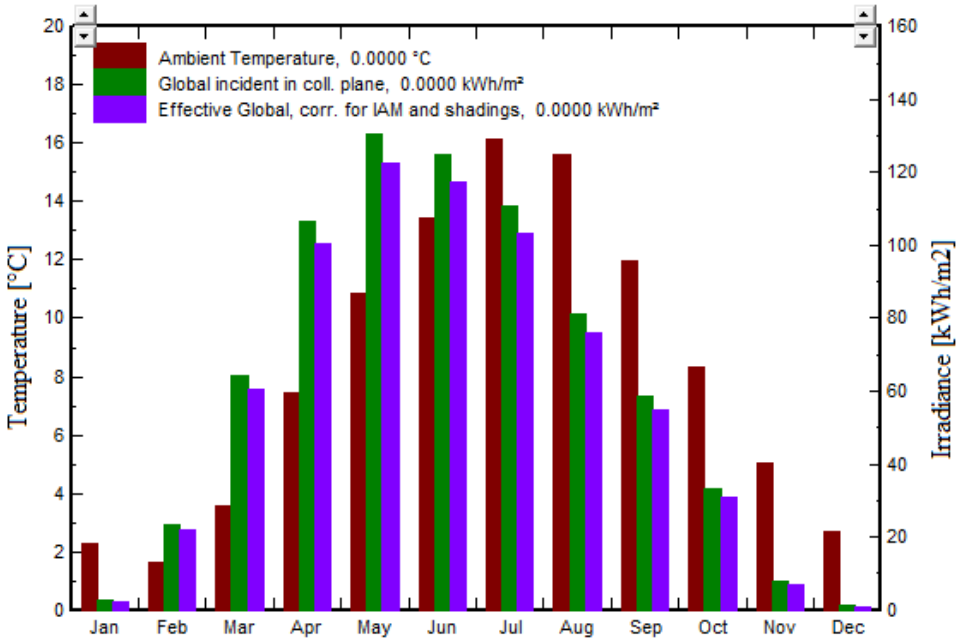

Figure 6.3: Ambient temperature on-site, global incident irradiation on collector plane and effective global irradiation corrected for array incidence loss and shadings.

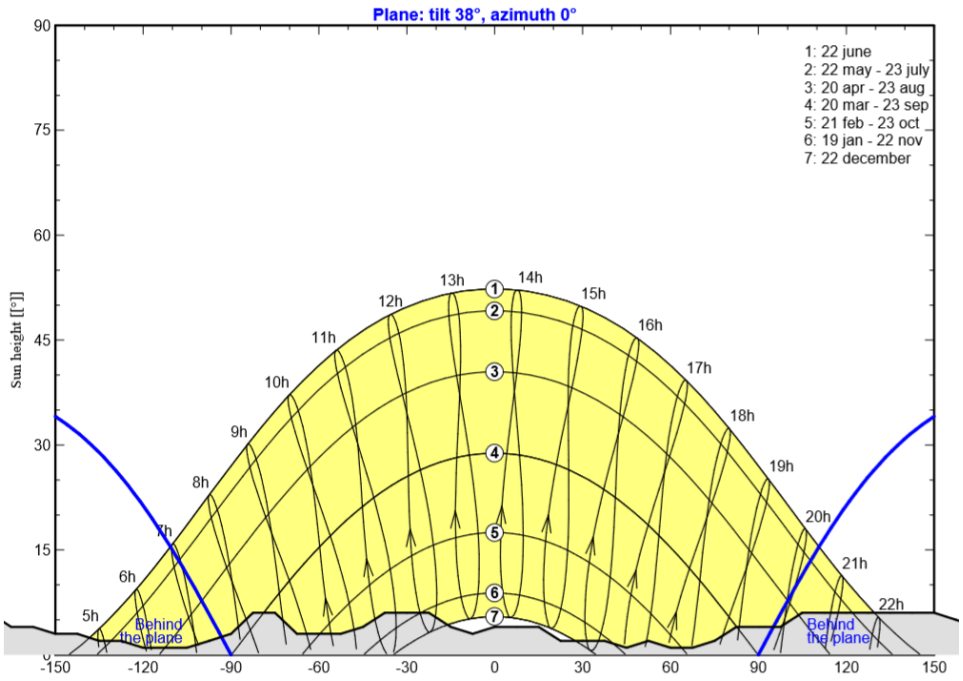

Figure 6.4: Horizon profile at the location of the power station

Table 6.2 illustrates the specific energy production of the exact copy of the system near Lavik at different locations. The only difference between the systems is the weather data and that the tilt angle is optimised for each location. From the table it is evident that the systems located in Barcelona and Cancún have a specific energy production of about two and a half times as much as in Lavik. The table also shows that the systems located in Oslo and Tromsoe have a specific energy production about one third higher than at Lavik.

Table 6.2: Specific energy production for the system at Lavik at different locations.

Location	Barcelona	Cancún	Lavik	Oslo	Tromsoe
Specific energy production [kWh/kWp/year]	1 643	1703	636	897	853

Figure 6.1 and Figure 6.2 shows that the energy production per square meter and energy delivered to the grid in November, December, and January is very low, which is due to the low sun height and few hours of sunlight during these months, as illustrated in Figure 6.4. The energy production and delivered energy increases rapidly from January through May, where it peaks, before it decreases gradually through December. The energy production and energy delivered to the grid peaks in May, which might seem strange at first glance due to a higher number of sun hours in June. However, since the system is designed for a maximum annual yield, there will be more hours of irradiation falling perpendicular to the collector plane in May than in June, as shown inFigure 6.3, resulting in higher power production, as discussed in Subsection 2.3.4. In addition, the temperature is higher in June than in May, which decreases the efficiency of the modules, as mentioned in Subsection 2.3.6. From Figure 6.3 it is clear that the temperature is approximately two degrees Celsius higher in June than in May, which corresponds to a 0.6 % relative decrease in efficiency, as discussed in Subsection 2.3.6.

Further on, the effective global irradiation is generally lower than global incident irradiation in collector plane due to correction of array incidence loss and shadings. The effective global irradiation varies throughout the year because of the variation of array incidence loss due to varying incidence angles, and because of shadings due to the varying horizon profile and sun height.

As mentioned in Section 4.3, MF Ampere consumes 1 836 MWh annually, corresponding to 153 MWh per month. The power station produces 2 046 MWh/year, hence an excess amount of energy equal to 210 MWh will be produced. By looking at Figure 6.2, it is evident that energy delivered to the grid is less than 153 MWh from October through February, and greater than 153 MWh from March through September. To cope with the shortage of energy during the

winter and excess energy during summer, an agreement with the local power company can be made to ensure exchange of energ. The excess energy can be sold to the power company or function as a compensation for the expensive energy prices during winter. In areas where pumped hydroelectric storage is unavailable, the excess energy could be stored in batteries or by hydrogen storage systems. However, if the battery package needs to be able to store the energy needed by MF Ampere throughout the winter, it needs to be around 600 MWh. A battery of this size has never been made, and it is about five times as big as the biggest battery in the world[1]. Therefore, it is not a realistic option. But, a smaller battery could be used to ensure that there is enough energy to charge the ferry when it lies at the ferry landing. This is crucial in areas with a weak grid. Such a battery should at least have a capacity equal to or greater than the capacity of the charger.

The reason the system is slightly oversized is to ensure that the power station produces enough energy to supply MF Ampere even for years with a high amount of cloudy days. The excess energy will vary for every year due to varying operating conditions for both the power station and the ferry. Its important to note that excess energy is calculated based on a consumption of 150 kWh per passage for MF Ampere, but this number will, in reality, fluctuate around 150 kWh depending on wind and ocean current velocity and direction. In addition, the number of passengers and vehicles aboard the ferry will also affect the energy consumption.

Since the power station site outside Lavik is close to the sea, reflection from water will increase the power output of the system. Anywhere between 5 % and 22 % can be reflected from the water, as discussed in Subsection 2.3.5. Moreover, reflection from snow can also contribute to increased power output on snow cover days, as mentioned in Subsection 2.3.5. The amount of reflected light from snow varies between 45-70 % for old snow cover and 80-90 % for fresh snow cover. For optimal increase in power output, the angle between reflected light and module surface should be equal to 90°, as mentioned in Subsection 2.3.4. The system was first simulated with an albedo of 0.2 for every month of the year, giving an energy output of 2 046 MWh/year. Then, the albedo was set to 0.82, that of fresh snow, during December, January, and February. For November and March the albedo was set to that of wet snow cover at 0.65, and 0.2 for the remaining months. This increased the energy output of the system by 9 MWh/year, reaching a total energy production of 2 055 MWh/year. Hence, by implementing the albedo for snow, the energy output of the system increased with 0.4 %. If the installed PV modules were bifacial instead of monofacial, the energy output could be increased by an additional

1. Currently, the world's leading battery is made by Tesla and has a capacity of 129 MWh [Godske, 2018].

5 – 30 % due to reflections from the surface behind the modules, as discussed in Subsection 2.3.2. However, the monofacial modules were preferred over the bifacial modules due to a lower cost per watt.

In Section 4.3, the idea of installing PV modules on a framework above the weather deck of MF Ampere was introduced. The available installation area was estimated to be 1 224 m^2. If PV modules were installed on this area, the system could produce enough energy to cover approximately 10 % of the annual consumption. For this scenario, there would be more loss due to shading, as the ferry would be shaded by the mountains above Oppedal at a certain distance from Oppedal and when the ferry lies at the ferry landing. However, the time spent at the ferry landing in Oppedal could be minimized in order to better utilize power production from the PV modules.

As mentioned in Section 4.3, MF Ampere is fully electric and has a yearly consumption of 1 836 MWh/year. If MF Ampere used MGO as fuel and had the same annual consumption mentioned above, it would emit 1 119 960 $kgCO_2$/year. The average CO_2 emission from new fossil fuel and hybrid cars in Norway in 2018 are estimated to emit 1 342 $kgCO_2$ over a year [OFV, 2018] [Statistics Norway, 2018]. Thus, by MF Ampere being fully electric, the amount of CO_2 emissions avoided each year equals 835 annual car equivalents. These numbers only regard the consumption of fuel. If the life-cycle analysis (LCA), which includes emission from all stages of the process, are taken into consideration the differences in emission between fossil fuel and renewable energy will be highlighted even more. The LCA for gas gives an emission of 477 gCO_2/kWh, coal emits 979 gCO_2/kWh and oil emits 800 gCO_2/kWh [Andrews and Jelley, 2013] [Andrews and Jelley, 2017]. For hydro power, the LCA gives an emission of 8 gCO_2/kWh and solar PV LCA gives 44 gCO_2/kWh. The LCA of gas and oil are 60 and 100 times greater than the LCA of hydro power, respectively. For solar PV, the LCA of gas and oil are 11 and 18 times higher, respectively. In other words, the LCA of hydro power is only 1.6 % and 1 % of gas and oil LCA, respectively. While the LCA of solar PV is 9.2 % and 5.5 % of the LCA of gas and oil, respectively. Thus, by going from gas and oil fuels to power generated from hydro power plants and solar PV, the LCA emission could be reduced by 90-99 %.

To manufacture PV modules, a certain amount of energy is required, which mainly comes from fossil fuels [Andrews and Jelley, 2017]. PV modules will therefore have an associated CO_2 emission. However, if the energy required to manufacture PV modules came from renewable energy sources, the associated CO_2 emission would be greatly reduced. It would not equal zero since renewable energy sources also have LCA emissions. The time it takes for the PV modules to produce the amount of energy it took to manufacture them is called the energy payback time (EPBT). With the present efficiencies, the EPBT in Northern

Europe is estimated to be 2.5 years, while it is estimated to be 1.5 years in Southern Europe. The break-even point (BEP) is the point where the total costs and total revenue are equal. In Lavik, the energy bought from the grid costs approximately 1.0 NOK/kWh, whereas the energy cost from the PV power plant is calculated to be 1.25 NOK/kWh. This leads to a loss of 511 kNOK/year, and the system will never reach a BEP. The system is therefore not economically feasible. If the system were located in Tromsoe or Oslo it would still have an absent BEP due to the low grid energy cost. The energy cost for the PV power stations is calculated based on a lifetime of 25 years. However, it can have a lifetime of 30 – 40 years, resulting in a lower energy cost and possibly a break-even point. It is important to note that the Norwegian grid energy prices are low since it is generated by hydro power. In countries where most of the grid power comes from fossil fuel, the PV systems have a huge potential with its low energy cost and low emissions.

Table 6.2 is included in this thesis to illustrate the differences between three locations in Norway. The table shows that the same system situated at Lavik would increase its specific energy production by 34 % and 41 % if located in Tromsoe and Oslo, respectively. This shows that the weather in Lavik is not at all optimal for power production from a PV power station, and that other places is Norway is far more suitable. In addition, the table shows the specific energy production of the system in Lavik situated in Barcelona and Cancún. If the system were located in Barcelona and Cancún, the specific energy production would increase by 158 % and 167 %, respectively. These two locations were chosen just to get an idea of the specific energy production around The Mediterranean Sea and The Mexico Gulf.

If 30 % of the investment costs for the PV power station in Lavik were received as incentives from Enova, the investment costs would be 22.1 million NOK for the investor. The corresponding energy cost would be 0.92 NOK/kWh, leading to a break-even point of 135 years. As the PV system might have a lifetime of 30 – 40 years, the BEP of the system will never be reached, and the system will not be economically feasible. In order for the system to have a BEP of 40 years, the energy cost from the PV system needs to be 0.73 NOK/kWh or lower.

Figure 5.1 shows that the expected efficiency of commercial n-type back contact monocrystalline Si-cells are 25.5 % in 2028. These cell's expected efficiency are 26.4 % higher than the monocrystaline Si-cells used in the simulations. In addition, the total system costs for utility-scale PV systems is predicted to drop by 53 % by 2025, as discussed in Subsection 3.3.1. The total system cost reduction should be greater in 2028, however, it is assumed to be 53 % in 2028. Based on this, the system at Lavik could produce 2 587 MWh/year with an energy cost of 0.59 NOK/kWh. This corresponds to an estimated BEP of 14 years.

6.2 PV Array on Edda Passat

This section presents the results obtained from the simulation done on the wind-farm support vessel Edda Passat. The results from the horizontal array will be presented first, then the results from the array with 15° tilt angle will be introduced. Further on, the results from the 35° tilted array will be presented, before presenting the results from the 80° tilted array. Finally, the results from each array will be combined, and presented as total production from the whole system on Edda Passat.

When Edda Passat operates at the Hornsea site, the front should be oriented towards the wind and ocean current direction in order to maintain the same position as stable as possible. Since operating conditions vary continuously, it is impossible to choose a fixed orientation for Edda Passat to face. Thus, the amount of time it faces different orientations is estimated to be 21 % each for north, east and west, and 37 % for south. The estimations are implemented by defining the installation area to be 21 % for north, east and west facing PV modules and 37 % for south facing PV modules. These estimations are based on the fact that the optimal orientation is due south, as discussed in Section 5.2, and that the captain of the vessel can to some extend orient the ship towards south more than the other directions.

6.2.1 Horizontal PV Array

As discussed in Section 4.1, the horizontal PV array is estimated to cover an area of 246 m^2. Figure 6.5 illustrates the energy output from the array for each month throughout the year. The energy output increases rapidly from January through May, where it peaks at 30 kWh/m^2. Further on, it drops in June before increasing in July, and then decreases gradually through December, with the lowest energy output of 2.3 kWh/m^2.

The energy transmitted to the grid from the array for each month of the year is illustrated in Figure 6.6. From January through May the energy transmitted to the grid increases fast, and peaks at 7.3 MWh. Further on, it decreases in June, and then increases in July before experiencing a rapid decrease through December, with the lowest transmitted energy at 0.5 MWh.

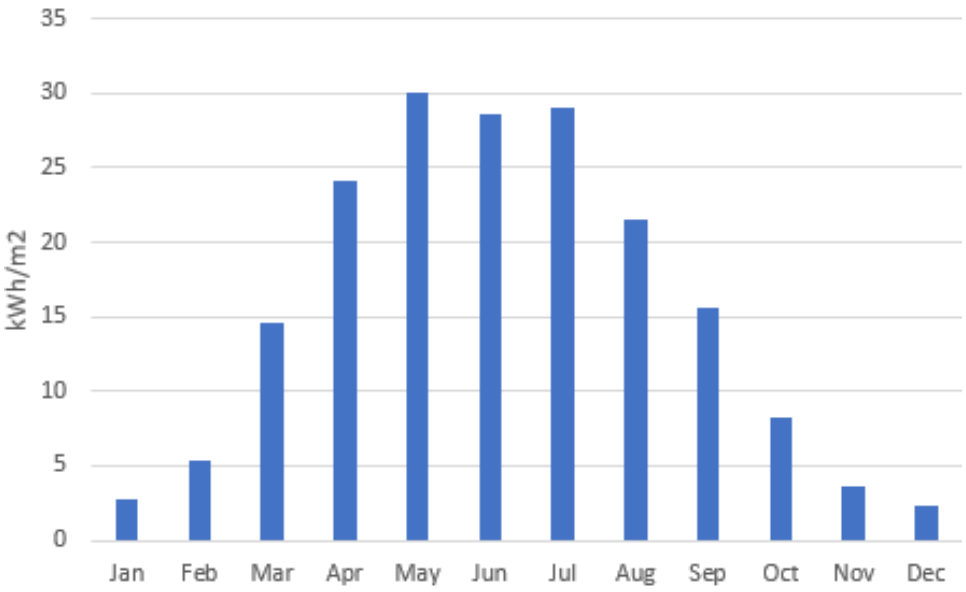

Figure 6.5: Energy output from horizontal PV array on Edda Passat for each month throughout the year.

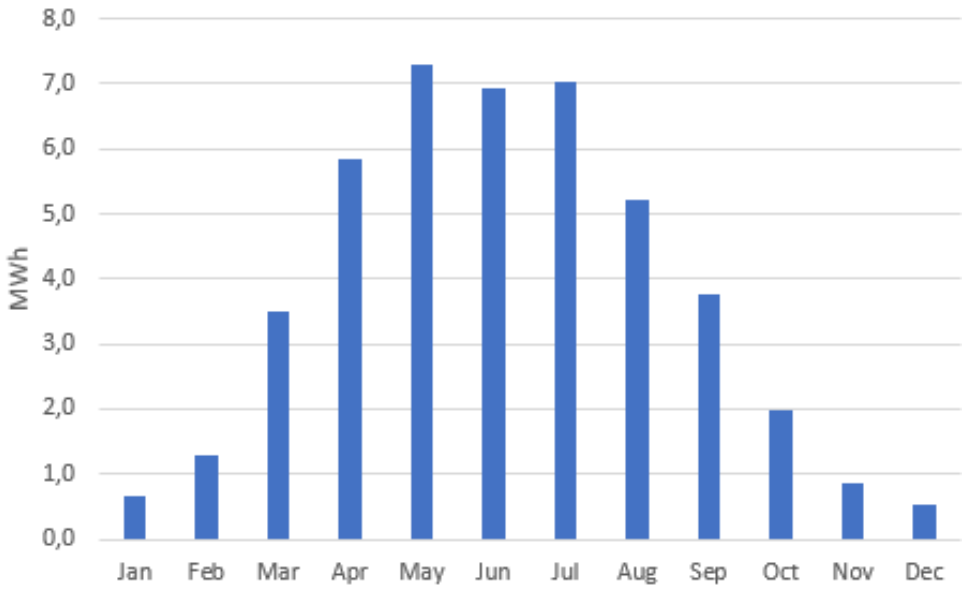

Figure 6.6: Energy transmitted to grid from horizontal PV array on Edda Passat for every month of the year.

6.2.2 PV Array Tilted with 15°

An estimated 10 % of the inclined surface discussed in Section 4.1 have an inclination of 15° where PV modules can be installed, which corresponds to 18.4 m^2. Figure 6.7 and Figure 6.8 illustrates the energy output from the array and energy transmitted to the grid for each month of the year, respectively. It is evident that both energy output and energy transmitted to grid increases gradually from January through May, and decreases from May to June. Then it increases in July, before decreasing through December. Energy output from the array is highest for the southward oriented modules from August to April, but in May, June and July the PV array facing East has the highest energy output. The energy output peaks in May at 31 kWh/m^2 for the eastward oriented array, and the lowest output occurs in December at 1.6 kWh/m^2 for the north facing array. For energy transmitted to the grid, the south facing array contributes most, followed by the east oriented, before the west and north oriented arrays. The highest amount of energy transmitted to the grid occurs in May at 0.54 MWh, while the lowest amount of transmitted energy appears in December at 0.05 MWh.

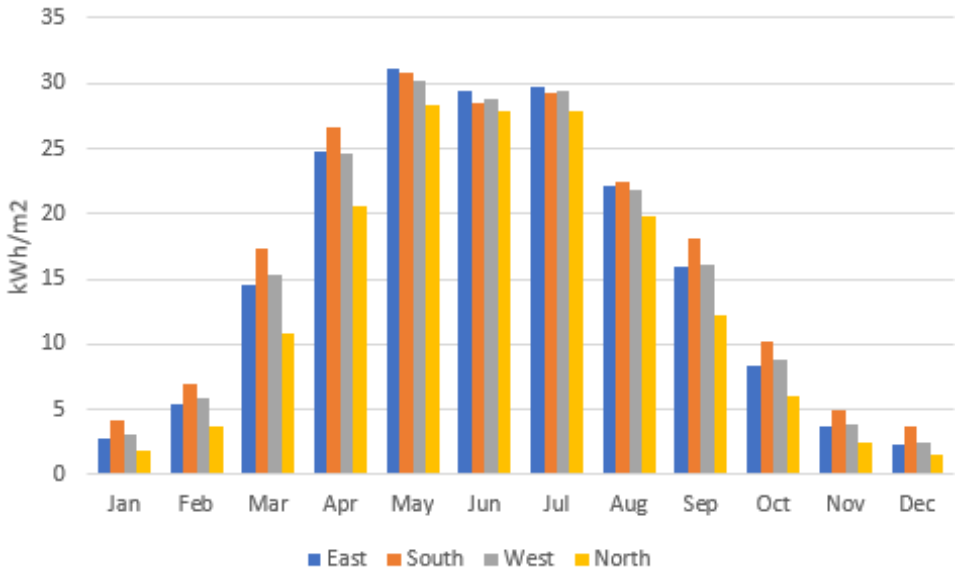

Figure 6.7: Energy output from 15° tilted PV array oriented in different directions on Edda Passat for each month throughout the year.

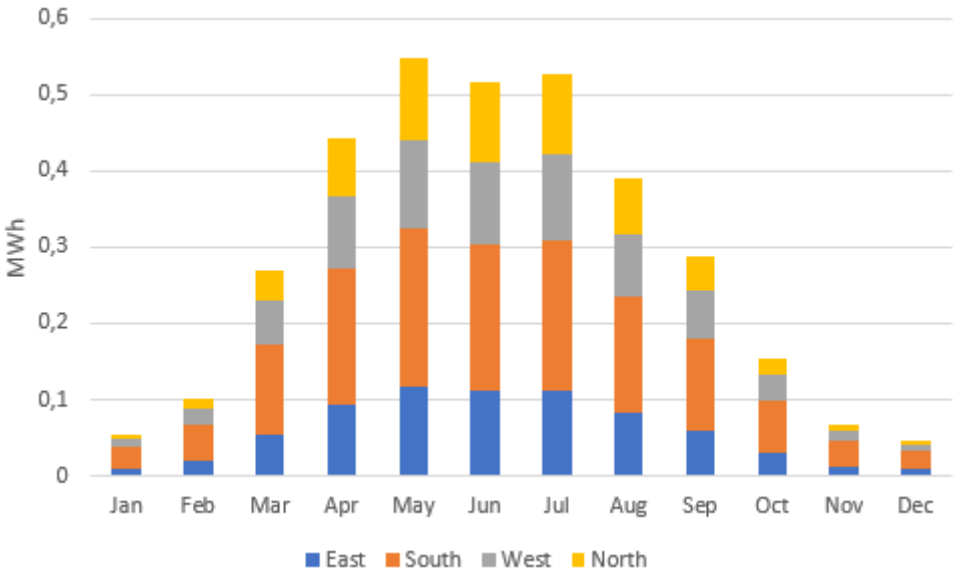

Figure 6.8: Energy transmitted to grid from 15° tilted PV array facing different directions on Edda Passat for every month throughout the year.

6.2.3 PV Array Tilted with 35°

The remaining inclined area, i.e. 90 %, is suitable for installation of PV modules with a tilt angle of 35°. Figure 6.9 illustrates the energy output per square meter from the array for each month of the year. By looking at the figure it is evident that the array facing south produces the highest amount of energy per square meter throughout the whole year, except for June, where the eastward oriented array has the highest production. The energy production is highest in May at 31 kWh/m^2, south facing array, and lowest in December at 1.5 kWh/m^2, north oriented array.

Figure 6.10 presents the energy transmitted to grid for each month throughout the year, respectively. The grid transmitted energy increases from January to May, where it peaks at 4.6 MWh, and then decreases in June. Further on, it increases again in July, before decreasing through December, where the lowest values throughout the year occurs at 0.5 MWh.

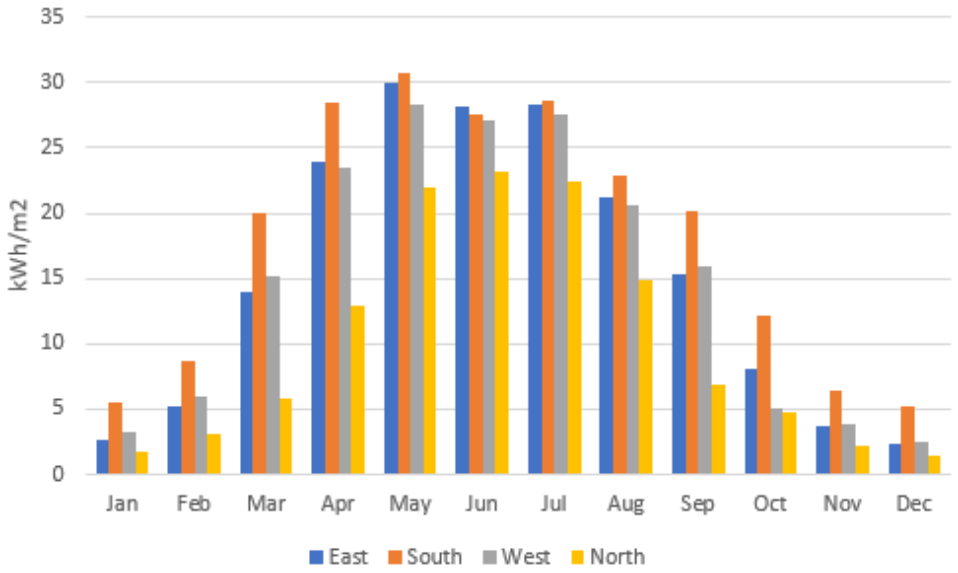

Figure 6.9: Energy output from 35° tilted PV array on Edda Passat oriented in different directions for each month throughout the year.

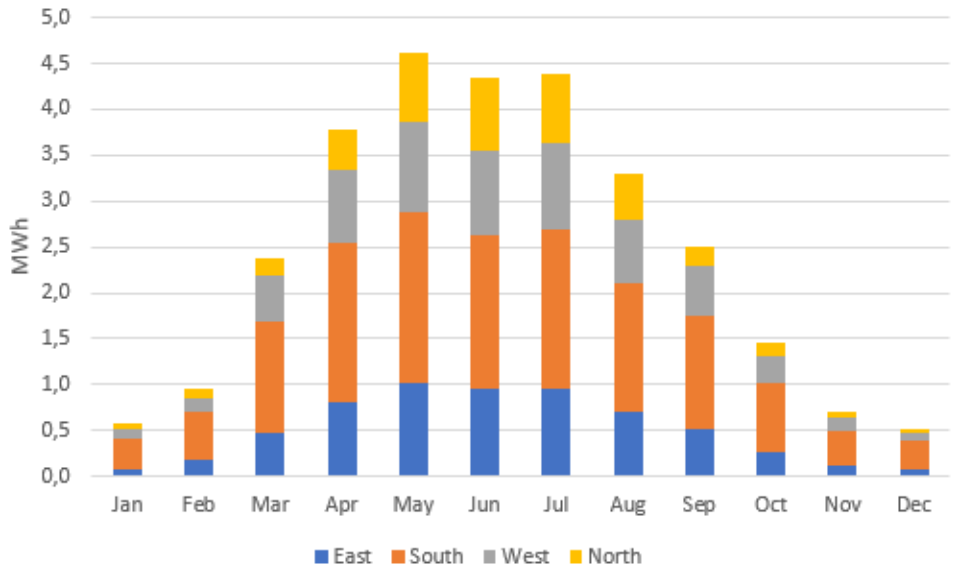

Figure 6.10: Energy transmitted to grid from 35° tilted PV array on Edda Passat facing different directions for every month throughout the year.

6.2.4 PV Array Tilted with 80°

The PV modules installed with a tilt angle of 80° can be mounted on both sides of the hull from the bridge to the front of the ship. However, irradiation will only hit one of the sides at a time. For these modules, the estimated time they face east is 37 %, and the estimated time they face south, west and north is 21 %. Figure 6.11 illustrates the energy output from the PV arrays facing different directions. The figure shows that the array facing south has the highest production per square meter from August through May, but in June and July the array oriented eastward has the highest production.

Figure 6.12 illustrates energy transmitted to the grid for the PV arrays facing different directions throughout the year. By looking at the figure it is evident that the transmitted energy increases rapidly from January to May, peaking at 0.75 MWh. Further on, it decreases slightly in June, before increasing in July, and then decreases to the lowest point in December at 0.1 MWh.

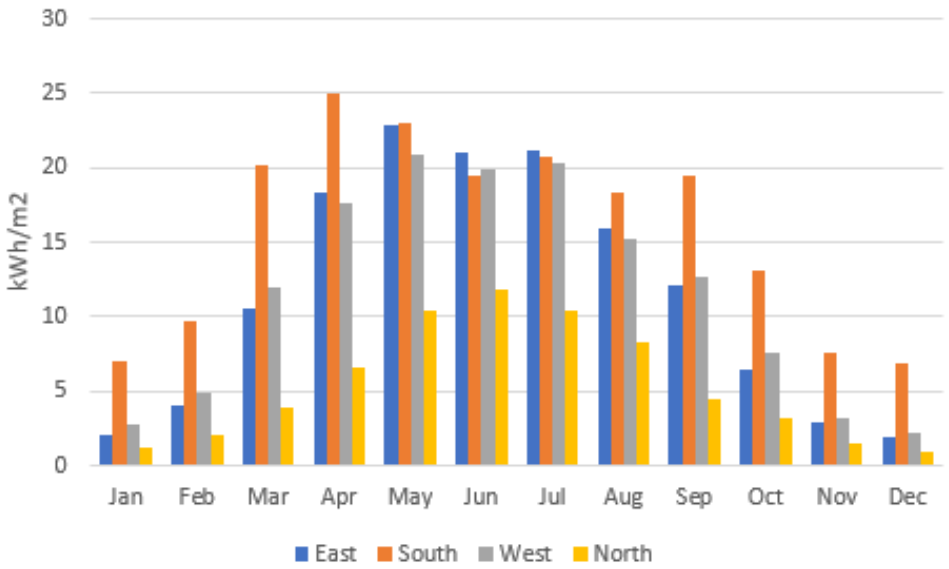

Figure 6.11: Energy output from 80° tilted PV array facing different directions on Edda Passat for each month throughout the year.

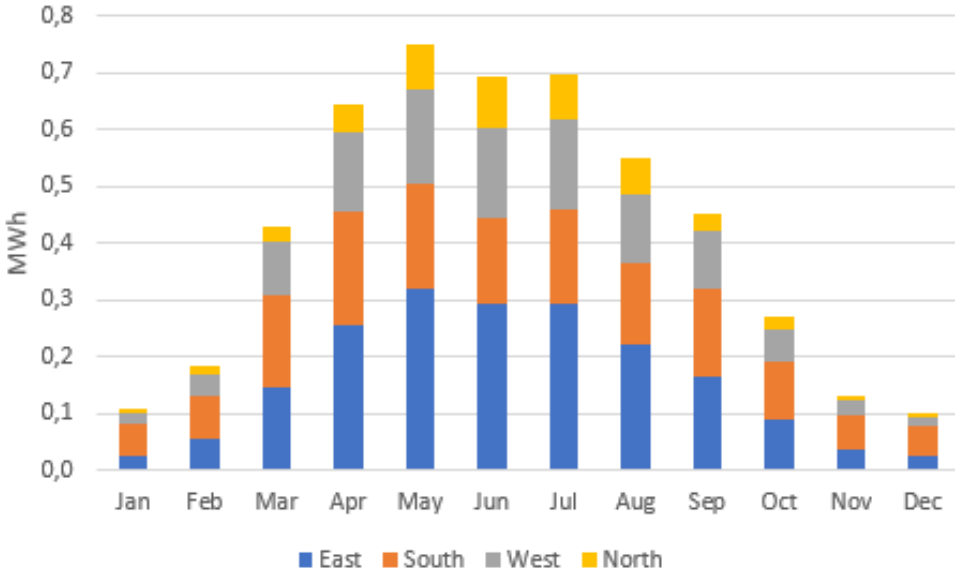

Figure 6.12: Energy transmitted to grid from 80° tilted PV array oriented in different directions on Edda Passat for every month throughout the year.

6.2.5 Total PV Array

The total PV array comprises of the horizontal, 15°, 35° and 80° tilted PV arrays. Out of the total area covering 508 m^2, the horizontal array covers 246 m^2, the 15° tilted array occupies approximately 18 m^2, the 35° tilted array covers around 166 m^2, while the 80° tilted array occupies 39 m^2.

The main results for the PV system on Edda Passat are illustrated in Table 6.3, and were achieved from simulation reports. The system produces 88 MWh/year, with a total nominal power of 103 kWp and has a specific energy production of 860 kWh/kWp/year. For the system, an annual average energy production per square meter is calculated to be 173 kWh/m^2/year. Table 6.3 shows that investment costs for such a system would lie around 1.1 million NOK, annuities at 44.5 kNOK and operation costs are estimated to be 10.2 kNOK/year. The energy cost is calculated by adding the annuities and operation cost and dividing the sum by produced energy, which gives 0.5 NOK/kWh.

Table 6.3: Main simulation results from the total PV array installed on Edda Passat

Main simulation results	
Total annual energy production	87.87 MWh/year
Total nominal power	103 kWp
Specific energy production	860 kWh/kWp/year
Average annual energy production	173 kWh/m^2/year
Investment	1 113 844 NOK
Annuities	33 415 NOK/year
Operation cost	10 223 NOK/year
Energy cost	0.5 NOK/kWh

The total energy output from the arrays are illustrated in Figure 6.13 for different tilt angles throughout the year. In this figure, the energy produced by PV modules with different orientations are added together, with respect to estimated time facing that direction, in order to illustrate the total energy produced by modules with same tilt angle. The figure shows that the PV array with a tilt angle of 15° produces the highest amount of energy per square meter from March through October. While the PV array with a tilt angle of 35° produces the highest energy output from November through February.

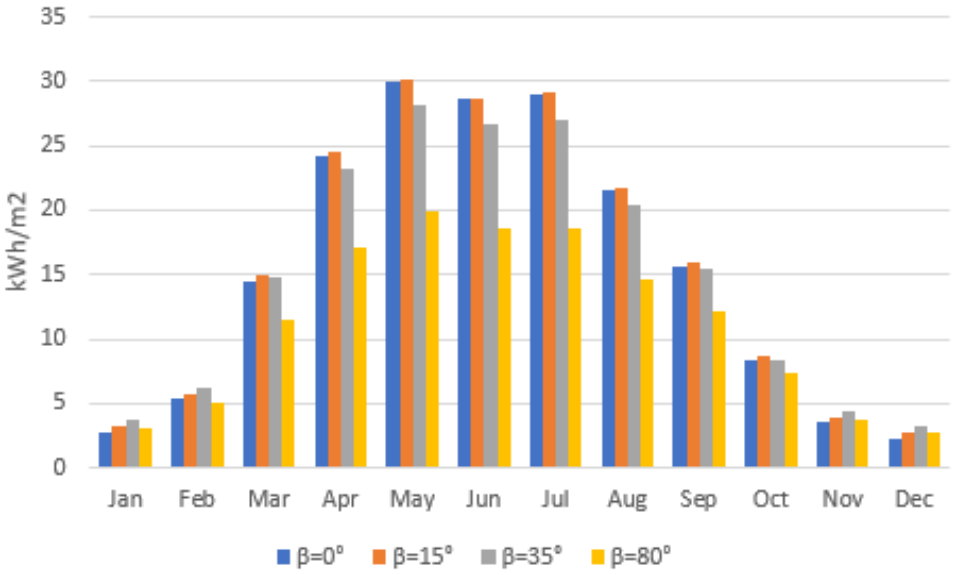

Figure 6.13: Energy output from PV arrays with different tilt angles on Edda Passat for each month throughout the year.

Figure 6.14 illustrates the total energy transmitted to the grid from arrays with different tilt angles for each month throughout the year. From the figure it is evident that total energy transmitted to the grid increases from January to May, peaking at 13 MWh, and then decreases slightly in June. Further on, it increases in July before it decreases through December where the lowest transmitted energy lies at 1.3 MWh.

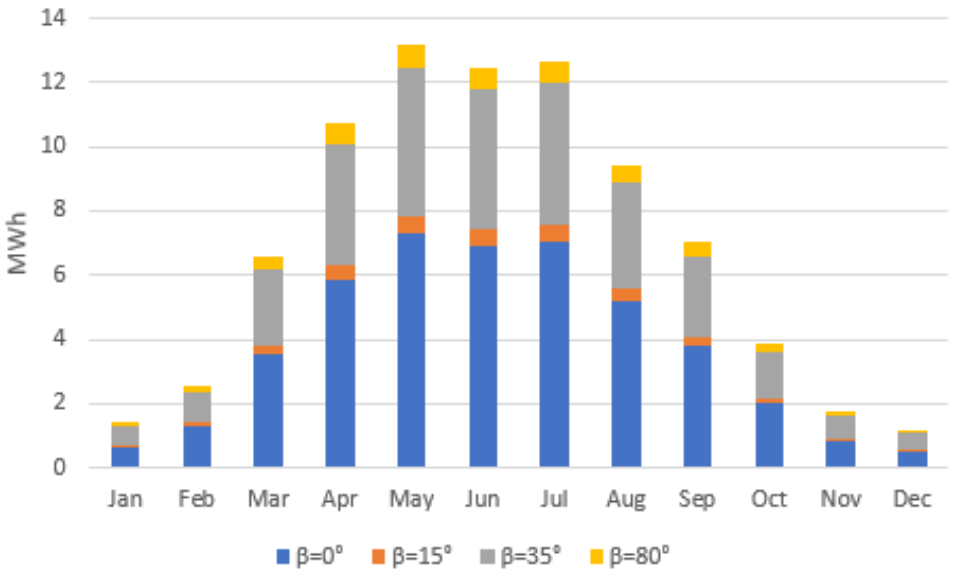

Figure 6.14: Total energy transmitted to grid from PV arrays with different tilt angles on Edda Passat for each month throughout the year.

From Figure 6.13 it is evident that the PV arrays with a tilt angle of 0°, 15° and 35° produce approximately the same amount of energy throughout the year. The figure shows that the PV arrays with $\beta = 0°$ and $\beta = 15°$ have a slightly higher energy production from April to September than the ones with $\beta = 35°$. This is due to more irradiation falling perpendicular, or close to perpendicular, to the plane for $\beta = 0°$ and $\beta = 15°$ than $\beta = 35°$. However, from November through February, the energy production from the PV array with a tilt angle of 35° is slightliy higher than the others.

Figure 6.13 also shows that energy production from the PV array with $\beta = 80°$ is significantly lower during the period March to September than the other three arrays. The reason being that the irradiation falling on the PV module surface is far from perpendicular. Whereas from October through February, it produces almost the same amount of energy as the arrays with $\beta = 0°$, $\beta = 15°$ and $\beta = 35°$. The PV arrays with tilt angle 0°, 15° and 35° have a energy production that is approximately 30 % higher, on average, than the PV arrays

with a tilt angle of 80°. A ship designer should therefore try to design the ship with areas suitable for installation of PV modules with angles between 0 – 35° to the horizontal.

The total energy production from the PV array on Edda Passat is 88 MWh/year, which corresponds to 2.86 % of the yearly consumption. In terms of fuel savings, this corresponds to 44.6 mt of MGO saved each year. Moreover, with an energy cost from the PV system of 0.5 NOK/kWh, the annual produced energy will correspond to 44 kNOK/year. For an engine consuming MGO, the energy cost is 1.97 NOK/kWh for a Tier III regulated engine, as discussed in Section 3.2, corresponding to 173 kNOK/year. By using energy from the PV system instead of burning MGO, the ship owners can save 129 kNOK/year. Hence, the BEP of the PV system is 8.6 years. Edda Passat will operate in the Hornsea zone located outside of England, and the PV system is estimated to have an EPBT of 2 years.

In addition, the Bergen C25:33L engine emits 610 gCO_2/kWh, whereas the PV system emits 44 gCO_2/kWh. The PV system on Edda Passat will therefore contribute to a reduction in CO_2 emissions by 49.7 $mtCO_2$/year. This is equivalent to the annual CO_2 emissions from 37 cars. Further on, the life-cycle analysis for gas and oil are 11 and 18 times higher than solar PV, respectively, as discussed in Section 6.1. Thus, the LCA could be reduced by around 90 %.

Figure 5.1 shows that the expected efficiency of commercial n-type back contact monocrystalline Si-cells are 25.5 % in 2028. These cell's expected efficiency are 26.4 % higher than the monocrystaline Si-cells used in the simulations. In addition, the total system costs for utility-scale PV systems is predicted to drop by 53 % by 2025, as discussed in Subsection 3.3.1. Since the system on Edda Passat is not utility-scale, this cost reduction potential is slightly inaccurate, however, a cost reduction of 53 % by 2028 will be assumed to give an idea of how much better the system could be in 10 years. Based on this, the system on Edda Passat could produce 111 MWh/year with an energy cost of 0.24 NOK/kWh in 2028.

/7

Conclusion

In conclusion, the power system located near Lavik produces 2 046 MWh/year with an energy cost of 1.25 NOK/kWh. Further on, the system located near Lavik has a specific energy production of 636 kWh/kWp/year. If the system was located in Tromsoe or Oslo, it would increase its specific energy production by 34 % and 41 %, respectively. If it was located in Barcelona or Cancún it would increase its specific energy production by 158 % and 163 %, respectively. For the PV power station located near Lavik, the energy payback time is estimated to be 2.5 years, while there is an absent of a break-even point.

The PV power system on Edda Passat produces 88 MWh/year, which accounts for 2.86 % of annual consumption, and it has a specific energy production of 860 kWh/kWp/year. For this system, the energy cost is calculated to be 0.5 NOK/kWh. Further on, by using energy from the PV system instead of burning MGO, an amount of 129 kNOK can be saved each year. This corresponds to a system BEP of 8.6 years. For a system located outside of England, the EPBT is estimated to be 2 years. Moreover, by installing a PV system, Edda Passat could contribute to a reduction in CO_2 emissions by 50 mt/year. In other words, the equivalent of the annual CO_2 emission from 37 cars. For both systems, the life-cycle analysis emissions could be reduced by 90-95 % by using power from solar PV instead of oil and gas.

The future potential of solar PV is promising with an expected increase in efficiency of 26.4 % for monocrystalline Si-cells over the next 10 years, and a predicted total system cost reduction of 53 % by 2025. Based on these predictions, the system at Lavik could produce 2 587 MWh/year with an energy cost of 0.59 NOK/kWh. While the system on Edda Passat could produce 111 MWh/year with an energy cost of 0.24 NOK/kWh in 2028. This energy cost is only 12.5 % of the present MGO cost. These numbers shows that solar PV is an important part of power generation for future solutions in marine applications.

Further Work

To improve the study performed in this thesis, the following examples of further work are given:

- The simulation results can be improved by implementing the design of Edda Passat in *PVsyst*. The PV modules can then be placed on the suitable areas, causing *PVsyst* to account for shading from railing and different equipment installed on the weather deck.

- The wind and ocean current directions in the Hornsea zone could be mapped out in order to improve the estimated time Edda Passat is oriented in different directions. By doing so, the simulations for the PV system on Edda Passat would be more accurate.

- A cooling system could be integrated on both PV systems in order to increase the efficiency of the PV modules. An analysis of increased efficiency and costs related to the cooling system needs to be done in order to evaluate whether or not it is feasible.

A

Trends in Global Shipping

The numbers presented in the following figures are estimated using the bottom-up method which estimates a ships emission based on automatic identification system data [Smith et al., 2015]. It gives information about the vessels position, speed, draught and identification at a given time, and sends information every six seconds. These data are received by satellites and land-based stations and then processed and used to calculate emission from the ships.

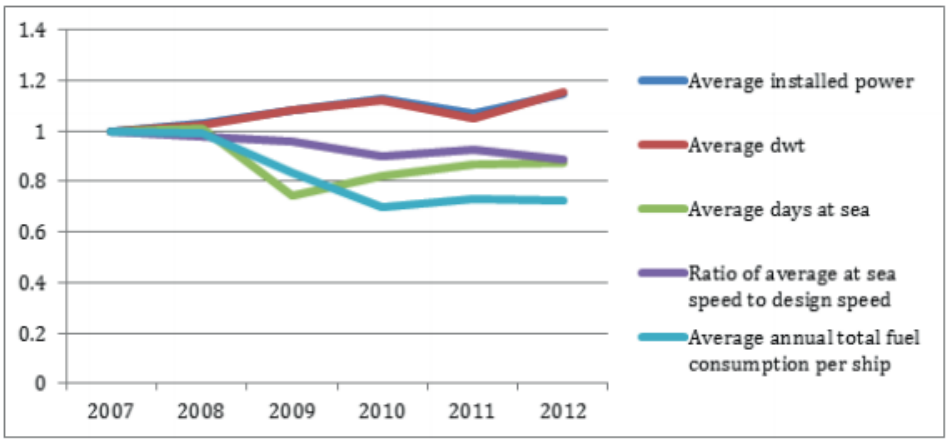

Figure A.1: Average trends in tanker sector from 2007–2012 [Smith et al., 2015]

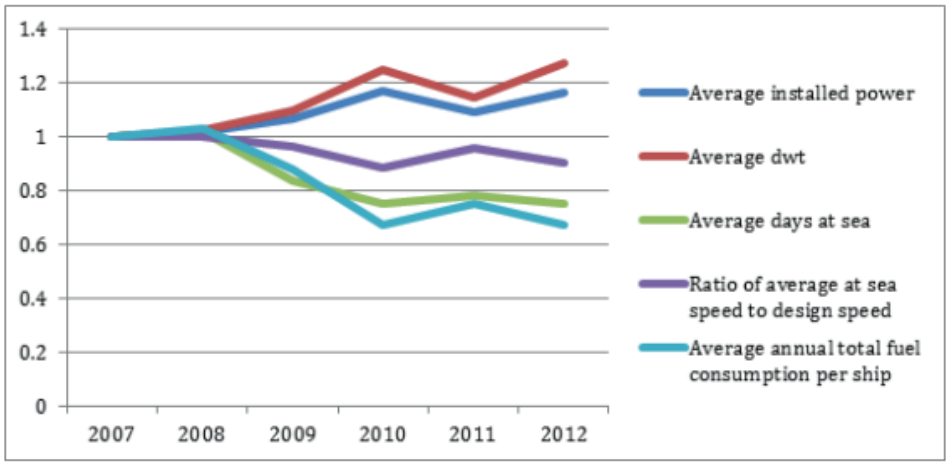

Figure A.2: Average trends in bulk carrier sector from 2007 – 2012 [Smith et al., 2015]

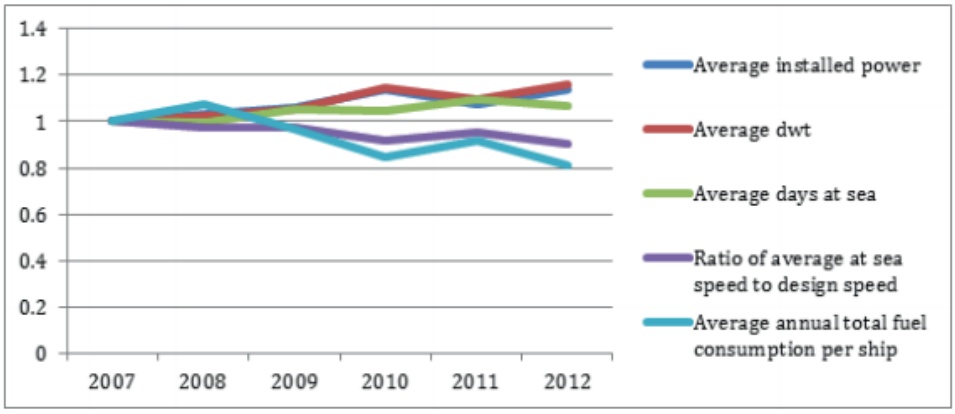

Figure A.3: Average trends in container ship sector from 2007 – 2012 [Smith et al., 2015]

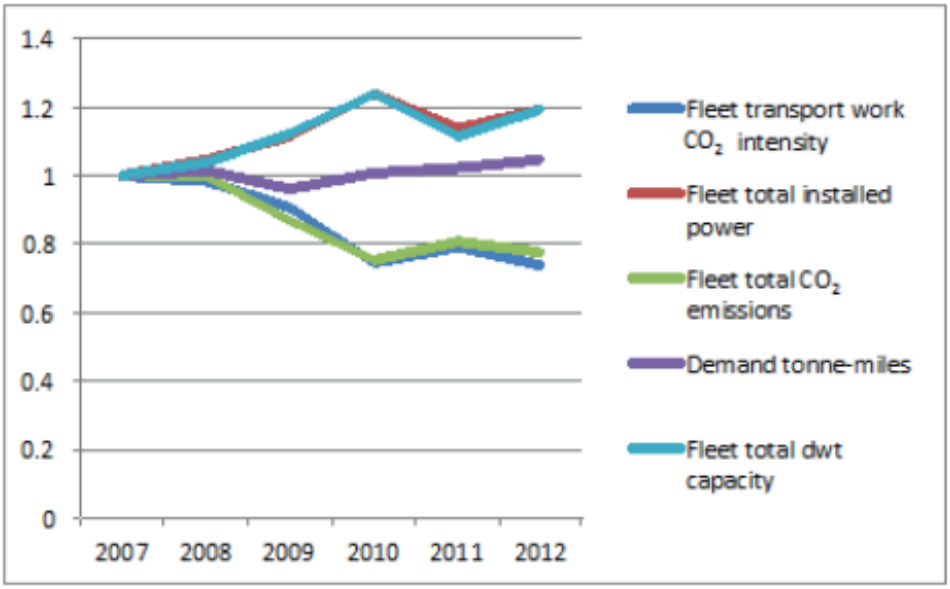

Figure A.4: Fleet total trends in tanker sector from 2007 – 2012 [Smith et al., 2015]

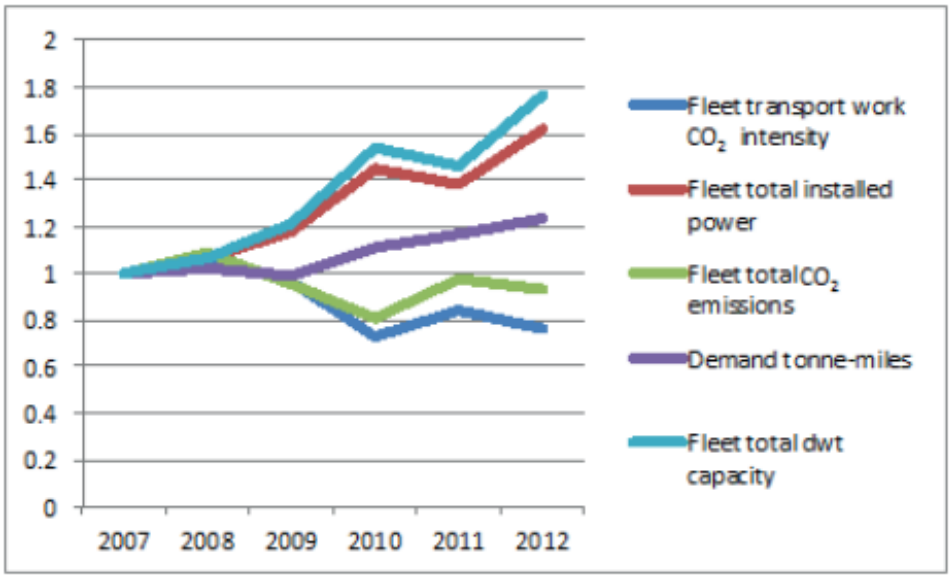

Figure A.5: Fleet total trends in bulk carrier sector from 2007 – 2012 [Smith et al., 2015]

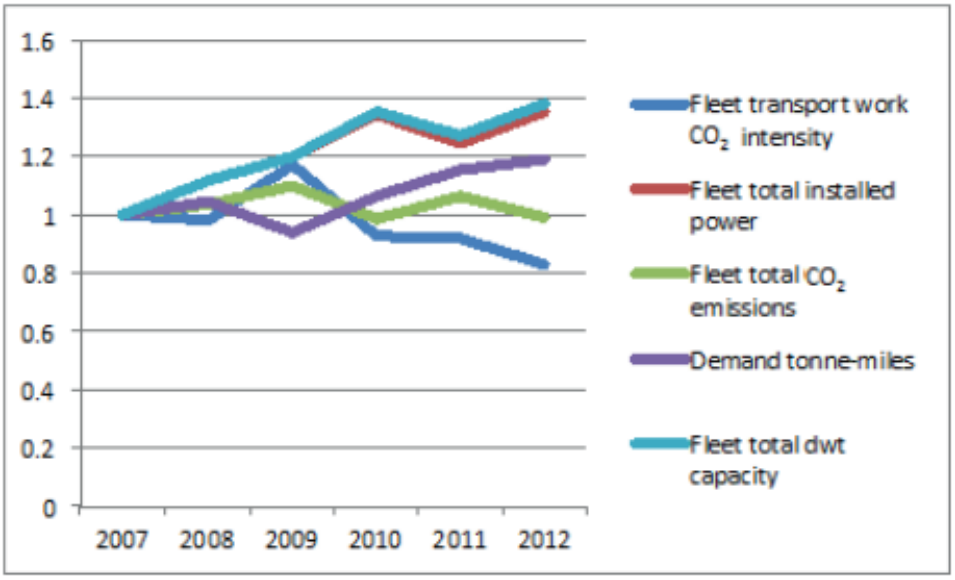

Figure A.6: Fleet total trends in container ship sector from 2007 – 2012 [Smith et al., 2015]

B

Suppliers of PV Modules

Table B.1 illustrates electrical and general data for the E20-435-COM PV module from *SunPower* [SunPower, 2016].

Table B.1: General and electrical data for the E20-435-COM PV module [SunPower, 2016].

E20-435-COM	
Parameters	Values
L/W/H	2067 mm / 1046 mm / 46 mm
Module area	2.162 m^2
Weight	25.4 kg
Operating temperature range	$(-40, 85)°C$
Number of cells in series	128
Maximum system voltage	1000 V
Nominal power P_N	435 W_P
Nominal voltage U_{MPP}	72.90 V
Nominal current I_{MPP}	5.97 A
Module efficiency	20.17 %
Power output per installed area	201.2 W/m^2
Area per kW	4.97 m^2/kW
Weight per kW	58.39 kg/kW
Temperature coefficient P_N	−0.35 %/°C
Temperature coefficient U_{OC}	−235.5 mV/°C
Temperature coefficient I_{SC}	2.6 mA/°C

C

Fuel and Cost Calculations

This appendix shows calculations of fuel cost, NOx emission and CO_2 emission for diesel and gas engines while operating under Tier II and Tier III regulations. In addition, it shows the estimated fuel and energy consumption per day for Edda Passat. The conversion ratios were taken from *Carbon Trust's* article *Energy and carbon conversions* [Carbon Trust, 2008].

C.1 MGO Costs

Listing C.1: Calculation of fuel and emission tax costs for diesel engines, implemented from MATLAB.

```
Cons = 200;                 % Consumption [gMGO/kWh]
P = 691.5*10^(-6);          % Price [USD/gMGO]
V = 7.7655;                 % Exchange ratio [NOK/USD]
E = 3.05;                   % CO2 emission [gCO2/gMGO]
Tax_D = 458*10^(-6);        % Domestic emission
                            % tax CO2 [NOK/gCO2]
N = 21.94*10^(-3);          % Domestic emission tax NOx
                            %                 [NOK/g]
N_2 = 9.6;                  % Tier II NOx emission [g/kWh]
N_3 = 2.4;                  % Tier III NOx emission [g/kWh]

% Fuel costs [NOK/kWh]
```

```
F_C = P*Cons*V

% Domestic CO2 emission tax [NOK/kWh]
D_C = E*Tax_D*Cons

% Tier II NOx emission tax [NOK/kWh]
C_N2 = N*N_2

% Tier III NOx emission tax [NOK/kWh]
C_N3 = N*N_3

% Results
F_C = 1.0740

D_C = 0.2794

C_N2 = 0.2106

C_N3 = 0.0527
```

C.2 LNG Costs

Listing C.2: Calculation of fuel and emission tax costs for gas engines, implemented from MATLAB.

```
Cons = 8305;          % Consumption [kJ/kWh]
A = 52.64;            % Conversion ratio [kJ/g]
P = 7.2;              % Price [USD/MMBtu]
V = 7.7655;           % Exchange ratio [NOK/USD]
B = 52.64*10^(-6);    % Conversion ratio [MMBtu/g]
E = 450;              % CO2 emission [g/kWh]
Tax_D = 457;          % Domestic emission tax CO2 [NOK/mt
    ]
N = 21.94*10^(-3);    % Domestic emission tax NOx [NOK/g]
N_2 = 9.6;            % Tier II NOx emission [g/kWh]
N_3 = 2.4;            % Tier III NOx emission [g/kWh]

% Fuel costs [NOK/kWh]
F_C = (Cons/A)*P*V*B

% Domestic CO2 emission tax [NOK/kWh]
D_C = E*Tax_D

% Tier II NOx emission tax [NOK/kWh]
C_N2 = N*N_2
```

```
20
21 % Tier III NOx emission tax [NOK/kWh]
22 C_N3 = N*N_3
23
24 % Results
25 F_C = 0.4643
26
27 D_C = 205650
28
29 C_N2 = 0.2106
30
31 C_N3 = 0.0527
```

C.3 Energy Consumption Edda Passat

Listing C.3: Calculation of fuel and energy usage per day for Edda Passat, implemented from MATLAB.

```
1  % Edda Passat kWh consumed per day
2  s = 14;          % Service speed consumption [mt/day]
3  DP = 5;          % DP-operations [m3/day]
4  IP = 1;          % In-port [m3/day]
5  n = 0.4;         % Motor efficiency
6  dens = 0.86;     % Density MGO [mt/m3]
7  C = 5000;        % MGO consumption [kWh/mt]
8  Ceff = C*n;      % Effective MGO consumption [kWh/mt]
9
10 % Typical operation profile for a day
11 Os = 0.05;       % Operation service speed
12 Odp = 0.8;       % Operation DP-operations
13 Oip = 0.15;      % Operation In-port
14
15 EP_fuel = s*Os+DP*Odp*dens+IP*Oip*dens
16 EP_energy = (s*Os+DP*Odp*dens+IP*Oip*dens)*Ceff
17
18 % Fuel and energy usage for Edda Passat
19
20 EP_fuel = 4.269      % [mt/day]
21
22 EP_energy = 8538     % [kWh/day]
```

D

Simulation Report Lavik

This appendix shows a detailed report of the simulation results. The implemented report is produced by *PVsyst* upon completion of the simulation.

PVSYST V6.63		23/05/18	Page 1/6

Grid-Connected System: Simulation parameters

Project : **Lavik_final**

Geographical Site **Lavik** Country **Norway**

Situation Latitude 61.10° N Longitude 5.54° E
Time defined as Legal Time Time zone UT+2 Altitude 10 m
Monthly albedo values

	Jan.	Feb.	Mar.	Apr.	May	June	July	Aug.	Sep.	Oct.	Nov.	Dec.
Albedo	0.82	0.82	0.65	0.20	0.20	0.20	0.20	0.20	0.20	0.20	0.65	0.82

Meteo data: **Lavik** Meteonorm 7.1 (1991-2010), Sat=95% - Synthetic

Simulation variant : **Lavik. 2 sub arrays, 8000 sq.m. soiling loss 3%, summer, albedo**
Simulation date 23/05/18 12h55

Simulation parameters

Collector Plane Orientation Tilt 38° Azimuth 0°

Models used Transposition Perez Diffuse Perez, Meteonorm

Horizon Average Height 3.7°

Near Shadings No Shadings

PV Arrays Characteristics (2 kinds of array defined)

PV module Si-mono Model **SPR-E20-435-COM**
Original PVsyst database Manufacturer SunPower

Sub-array "Sub-array #2"

Number of PV modules	In series	10 modules	In parallel	370 strings
Total number of PV modules	Nb. modules	3700	Unit Nom. Power	435 Wp
Array global power	Nominal (STC)	**1610 kWp**	At operating cond.	1460 kWp (50°C)
Array operating characteristics (50°C)	U mpp	648 V	I mpp	2253 A

Sub-array "Sub-array #1"

Number of PV modules	In series	10 modules	In parallel	370 strings
Total number of PV modules	Nb. modules	3700	Unit Nom. Power	435 Wp
Array global power	Nominal (STC)	**1610 kWp**	At operating cond.	1460 kWp (50°C)
Array operating characteristics (50°C)	U mpp	648 V	I mpp	2253 A

Total Arrays global power Nominal (STC) **3219 kWp** Total 7400 modules
Module area **15999 m²** Cell area 14521 m²

Inverter Model **890GTS_1600**
Original PVsyst database Manufacturer Parker Hannifin
Characteristics Operating Voltage 545-1000 V Unit Nom. Power 1600 kWac

Sub-array "Sub-array #2" Nb. of inverters 1 units Total Power 1600 kWac
Sub-array "Sub-array #1" Nb. of inverters 1 units Total Power 1600 kWac

Total Nb. of inverters 2 Total Power 3200 kWac

PV Array loss factors

Array Soiling Losses			Loss Fraction	3.0 %
Thermal Loss factor	Uc (const)	29.0 W/m²K	Uv (wind)	0.0 W/m²K / m/s
Wiring Ohmic Loss	Array#1	4.8 mOhm	Loss Fraction	1.5 % at STC
	Array#2	4.8 mOhm	Loss Fraction	1.5 % at STC
	Global		Loss Fraction	1.5 % at STC
Module Quality Loss			Loss Fraction	2.5 %
Module Mismatch Losses			Loss Fraction	1.0 % at MPP

Grid-Connected System: Horizon definition

Project : **Lavik_final**

Simulation variant : **Lavik. 2 sub arrays, 8000 sq.m. soiling loss 3%, summer, albedo**

Main system parameters	System type	**Grid-Connected**		
Horizon	Average Height	3.7°		
PV Field Orientation	tilt	38°	azimuth	0°
PV modules	Model	SPR-E20-435-COM	Pnom	435 Wp
PV Array	Nb. of modules	7400	Pnom total	**3219 kWp**
Inverter	Model	890GTS_1600	Pnom	1600 kW ac
Inverter pack	Nb. of units	2.0	Pnom total	**3200 kW ac**
User's needs	Unlimited load (grid)			

Horizon

Average Height	3.7°	Diffuse Factor	0.97
Albedo Factor	100 %	Albedo Fraction	0.82

Height [°]	5.0	6.0	4.0	4.0	3.0	3.0	2.0	2.0	1.0	1.0	1.0	2.0	3.0
Azimuth [°]	-180	-173	-165	-158	-150	-143	-135	-128	-120	-113	-105	-98	-90
Height [°]	6.0	6.0	3.0	3.0	3.0	4.0	6.0	6.0	6.0	4.0	3.0	4.0	4.0
Azimuth [°]	-83	-75	-68	-60	-53	-45	-38	-30	-23	-15	-8	0	8
Height [°]	4.0	2.0	2.0	2.0	1.0	2.0	1.0	1.0	2.0	4.0	4.0	4.0	6.0
Azimuth [°]	15	23	30	38	45	53	60	68	75	83	90	98	105
Height [°]	6.0	6.0	6.0	6.0	6.0	6.0	5.0	4.0	4.0	5.0			
Azimuth [°]	113	120	128	135	143	150	158	165	173	180			

Horizon file (source is not a PVsyst format!)

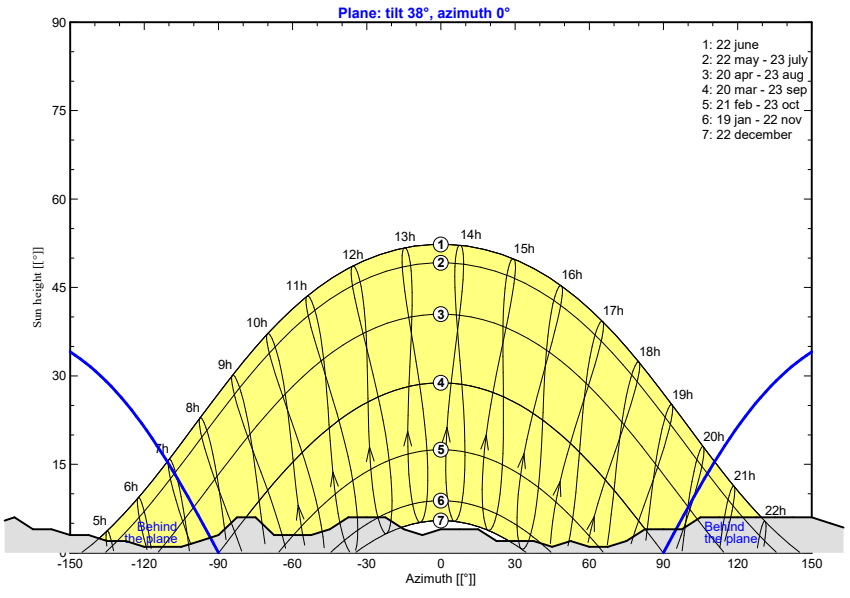

PVSYST V6.63		23/05/18	Page 4/6

Grid-Connected System: Main results

Project : **Lavik_final**

Simulation variant : **Lavik. 2 sub arrays, 8000 sq.m. soiling loss 3%, summer, albedo**

Main system parameters	System type	**Grid-Connected**		
Horizon	Average Height	3.7°		
PV Field Orientation	tilt	38°	azimuth	0°
PV modules	Model	SPR-E20-435-COM	Pnom	435 Wp
PV Array	Nb. of modules	7400	Pnom total	**3219 kWp**
Inverter	Model	890GTS_1600	Pnom	1600 kW ac
Inverter pack	Nb. of units	2.0	Pnom total	**3200 kW ac**
User's needs	Unlimited load (grid)			

Main simulation results

System Production	**Produced Energy**	**2055 MWh/year**	Specific prod.	638 kWh/kWp/year
	Performance Ratio PR	85.30 %		
Investment	Global incl. taxes	31567960 NOK	Specific	9.81 NOK/Wp
Yearly cost	Annuities (Loan 5.0%, 25 years)	2239824 NOK/yr	Running Costs	321900 NOK/yr
Energy cost		**1.25 NOK/kWh**		

Normalized productions (per installed kWp): Nominal power 3219 kWp

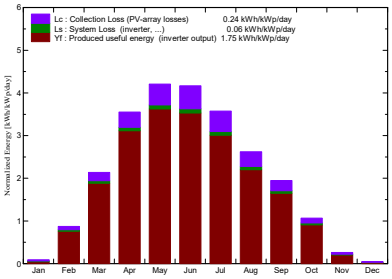

Performance Ratio PR

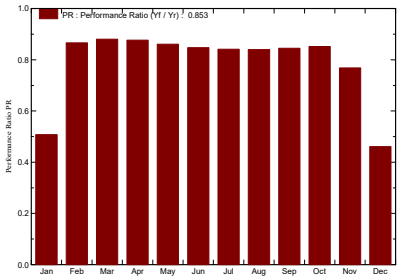

Lavik. 2 sub arrays, 8000 sq.m. soiling loss 3%, summer, albedo

Balances and main results

	GlobHor kWh/m²	DiffHor kWh/m²	T Amb °C	GlobInc kWh/m²	GlobEff kWh/m²	EArray MWh	E_Grid MWh	PR
January	3.1	3.09	2.28	2.8	2.1	6.1	4.5	0.508
February	14.3	11.14	1.60	24.5	22.6	71.5	68.2	0.866
March	45.5	29.04	3.56	66.3	62.0	193.9	187.9	0.881
April	89.2	50.09	7.42	106.6	100.2	308.7	300.7	0.877
May	122.8	70.70	10.83	130.4	122.5	371.2	361.6	0.861
June	123.8	64.32	13.44	125.0	117.3	350.5	340.8	0.847
July	112.4	79.36	16.13	110.8	103.3	308.9	300.2	0.841
August	75.7	53.71	15.61	81.3	75.9	227.1	219.7	0.840
September	48.1	33.70	11.98	58.4	54.7	164.9	159.1	0.845
October	22.6	17.68	8.34	33.1	30.9	94.9	90.7	0.852
November	5.3	4.48	5.01	7.8	7.0	21.3	19.4	0.768
December	1.6	1.53	2.66	1.5	1.0	3.0	2.2	0.461
Year	664.4	418.84	8.28	748.4	699.5	2122.1	2055.0	0.853

Legends:
GlobHor Horizontal global irradiation
DiffHor Horizontal diffuse irradiation
T Amb Ambient Temperature
GlobInc Global incident in coll. plane
GlobEff Effective Global, corr. for IAM and shadings
EArray Effective energy at the output of the array
E_Grid Energy injected into grid
PR Performance Ratio

PVSYST V6.63		23/05/18	Page 5/6

Grid-Connected System: Loss diagram

Project : **Lavik_final**

Simulation variant : **Lavik. 2 sub arrays, 8000 sq.m. soiling loss 3%, summer, albedo**

Main system parameters	System type	**Grid-Connected**		
Horizon	Average Height	3.7°		
PV Field Orientation	tilt	38°	azimuth	0°
PV modules	Model	SPR-E20-435-COM	Pnom	435 Wp
PV Array	Nb. of modules	7400	Pnom total	**3219 kWp**
Inverter	Model	890GTS_1600	Pnom	1600 kW ac
Inverter pack	Nb. of units	2.0	Pnom total	**3200 kW ac**
User's needs	Unlimited load (grid)			

Loss diagram over the whole year

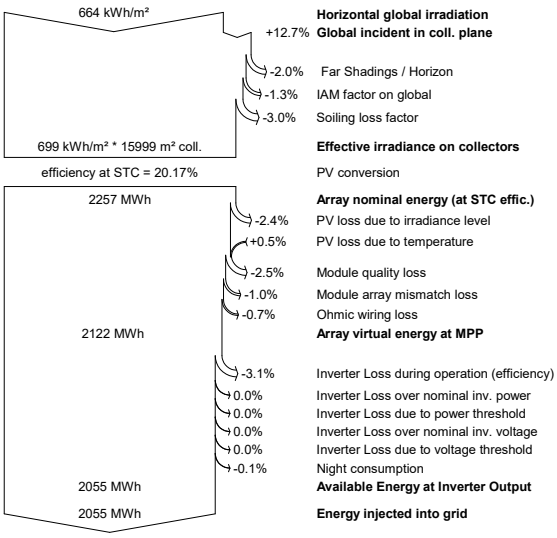

PVSYST V6.63		23/05/18	Page 6/6

Grid-Connected System: Economic evaluation

Project : **Lavik_final**

Simulation variant : **Lavik. 2 sub arrays, 8000 sq.m. soiling loss 3%, summer, albedo**

Main system parameters	System type	**Grid-Connected**			
Horizon	Average Height	3.7°			
PV Field Orientation	tilt	38°	azimuth	0°	
PV modules	Model	SPR-E20-435-COM	Pnom	435 Wp	
PV Array	Nb. of modules	7400	Pnom total	**3219 kWp**	
Inverter	Model	890GTS_1600	Pnom	1600 kW ac	
Inverter pack	Nb. of units	2.0	Pnom total	**3200 kW ac**	
User's needs	Unlimited load (grid)				

Investment

PV modules (Pnom = 435 Wp)	7400 units	3000 NOK / unit	22200000	NOK
Supports / Integration		522 NOK / module	3862800	NOK
Inverters (Pnom = 1600 kW ac)	2 units	50000 NOK / unit	100000	NOK
Settings, wiring, ...			1287600	NOK
Substitution underworth			0	NOK
Gross investment (without taxes)			**27450400**	**NOK**

Financing

Gross investment (without taxes)		27450400	NOK
Taxes on investment (VAT)	Rate 15.0 %	4117560	NOK
Gross investment (including VAT)		31567960	NOK
Subsidies		0	NOK
Net investment (all taxes included)		**31567960**	**NOK**
Annuities	(Loan 5.0 % over 25 years)	2239824	NOK/year
Annual running costs: maintenance, insurances ...		321900	NOK/year
Total yearly cost		**2561724**	**NOK/year**

Energy cost

Produced Energy	2055	MWh / year
Cost of produced energy	1.25	NOK / kWh

Bibliography

[4C Offshore Ltd, 2018] 4C Offshore Ltd (2018). Hornsea Project One Offshore Wind Farm. Last updated 01. Apr. 2018. http://www.4coffshore.com/windfarms/hornsea-project-one-united-kingdom-uk81.html. Accessed 03. Apr. 2018.

[Ahmed et al., 2016] Ahmed, S., Castelazzi, A., and Williams, A. (2016). Multi-source energy networks for cargo vessels. *Transactions on environment and electrical engineering*, 1.

[Al-Khazzar and Talib, 2015] Al-Khazzar, A. and Talib, E. (2015). Temperature Effect on Power Drop of Different Photovoltaic Modules.

[Andrews and Jelley, 2013] Andrews, J. and Jelley, N. (2013). *Energy Science - principles, technologies and impacts*. Oxford University Press, 2 edition.

[Andrews and Jelley, 2017] Andrews, J. and Jelley, N. (2017). *Energy Science - principles, technologies and impacts*. Oxford University Press, 3 edition.

[ARTTIC, 2018] ARTTIC (2018). New European research project to tackle the challenges of offshore wind farm O&M through new Service Operation Vessel concept. Published 22. Mar. 2018. urlhttp://www.arttic.eu/pages/posts/h2020-nexus-project-press-release-175.php. Accessed 10. May 2018.

[Bluegold Research, 2018] Bluegold Research (2018). Global LNG Prices. https://bluegoldresearch.com/global-lng-prices. Accessed 12. Apr. 2018.

[Bushong, 2016] Bushong, S. (2016). What kind of solar panels does NASA use? Solar Power World. https://www.solarpowerworldonline.com/2016/03/kind-solar-panels-nasa-use/. Accessed 24. Apr. 2018.

[Carbon Trust, 2008] Carbon Trust (2008). Energy and carbon conversions.

[Cefic & ECTA, 2011] Cefic & ECTA (2011). Guidelines for Measuring and Man-

aging CO_2 Emission from Freight Transport Operations.

[Enova, 2018a] Enova (2018a). Energi- og klimatiltak i skip. https://www.enova.no/bedrift/maritim-transport/energi--og-klimatiltak-i-skip/. Accessed 22. May 2018.

[Enova, 2018b] Enova (2018b). Om organisasjonen. https://www.enova.no/om-enova/om-organisasjonen/. Accessed 22. May 2018.

[Enova, 2018c] Enova (2018c). Utkast til utlysning 2018 - Frist 10.oktober! https://www.enova.no/pilot-e/utlysning-3---frist-10oktober/. Accessed 10. May 2018.

[EPRI, 2016] EPRI (2016). Bifacial Solar Photovoltaic Modules: Program on Technology and Innovation. Electric Power Research Institute. Palo Alto, California.

[European Commission, 2017] European Commission (2017). Photovoltaic Geographical Information System. http://re.jrc.ec.europa.eu/pvg_tools/en/tools.html#PVP. Accessed 25. Apr. 2018.

[Fairley, 2015] Fairley, P. (2015). How Rooftop Solar Can Stabilize the Grid. Published 21 Jan. 2015. https://spectrum.ieee.org/green-tech/solar/how-rooftop-solar-can-stabilize-the-grid. Accessed 09. May 2018.

[Finansdepartementet, 2018] Finansdepartementet (2018). Skatter, avgifter og toll 2018. https://www.statsbudsjettet.no/Statsbudsjettet-2018/Dokumenter/Budsjettdokumenter/skatter-avgifter-toll/Prop-1-LS-/Del-2-Narmere-om-forslagene-/9-Saravgifter-/. Accessed 12. Apr. 2018.

[Fraunhofer ISE, 2017] Fraunhofer ISE (2017). Photovoltaics Report. Fraunhofer Institute for Solar Energy Systems. Updated 26. feb. 2018.

[Godske, 2018] Godske, B. (2018). Verdens største litiumion-batteri har tjent millioner på få dager. Teknisk Ukeblad. Published 28. Jan. 2018. https://www.tu.no/artikler/teslas-megabatteri-har-tjent-millioner-pa-fa-dager/426738. Accessed 14. May 2018.

[Gudmestad, 2015] Gudmestad, O. T. (2015). *Marine Technology and Operations: Theory & Practice*, chapter 2. WIT Press.

[IEA, 2017] IEA (2017). Key World Energy Statistics. International Energy Agency. Paris.

[IEC, 2018] IEC (2018). Salt mist corrosion testing of photovoltaic (pv) modules. International Electrotechnical Comission.

[IMO, 2011] IMO (2011). IMO and the Environment. International Maritime Organization.

[IMO, 2018] IMO (2018). Nitrogen Oxide (NOx) - Regulation 13. London: International Maritime Organization. http://www.imo.org/en/OurWork/environment/pollutionprevention/airpollution/pages/nitrogen-oxides-(nox)-%E2%80%93-regulation-13.aspx. Accessed 10. Apr. 2018.

[IRENA, 2016a] IRENA (2016a). REmap: Roadmap for a Renewable Energy Future. Abu Dhabi: International Renewable Energy Agency.

[IRENA, 2016b] IRENA (2016b). The Power to Change: Solar and Wind Cost Reduction Potential to 2025. Abu Dhabi: International Renewable Energy Agency.

[IRENA, 2018] IRENA (2018). Renewable Power Generation Costs in 2017. Abu Dhabi: International Renewable Energy Agency.

[ITRPV, 2018] ITRPV (2018). International Technology Roadmap for Photovoltaic (ITRPV) Results 2017. Ninth Edition.

[Jordan et al., 2016] Jordan, D. C., Kurtz, S. R., VanSant, K., and Newmiller, J. (2016). Compendium of photovoltaic degradation rates. *Progress in photovoltaics: research and applications*, 24.

[Kobougias et al., 2013] Kobougias, I., Tatakis, E., and Prousalidis, J. (2013). PV Systems Installed in Marine Vessels: Technologies and Specifications. *Advances in Power Electronics*, pages 3–4.

[Kystverket, 2018] Kystverket (2018). Norgeskart. https://www.norgeskart.no.

[Norges Bank, 2018] Norges Bank (2018). EXCHANGE RATE FOR US DOLLAR (USD). https://www.norges-bank.no/en/Statistics/exchange_rates/currency/USD. Accessed 11. Apr. 2018.

[NTA, 2018] NTA (2018). NOx tax. http://www.skatteetaten.no/en/business-and-organisation/duties1/environment/nox-tax/. Accessed 23. Jan. 2018.

[offshoreWIND, 2017] offshoreWIND (2017). LOC Renewables Nets Hornsea Project One Contract. 17. Jul. 2017. https://www.offshorewind.biz/2017/07/

17/loc-renewables-nets-hornsea-project-one-contract/. Accessed 26. Mar. 2018.

[OFV, 2018] OFV (2018). Co2-utslippet. Opplysningsrådet for Veitrafikken AS. http://www.ofvas.no/co2-utslippet-b-i-l/category635.html. Accessed 21. May 2018.

[PV Education, 2017] PV Education (2017). Solar Cell Structure. http://www.pveducation.org/pvcdrom/solar-cell-structure. Accessed 22. Nov. 2017.

[PV Education, 2018a] PV Education (2018a). Air Mass. http://www.pveducation.org/pvcdrom/2-properties-sunlight/air-mass. Accessed 24. Jan. 2018.

[PV Education, 2018b] PV Education (2018b). Module structure. http://pveducation.org/pvcdrom/modules/modules-structure.

[PVsyst, 2014] PVsyst (2014). PVsyst 6 help. http://files.pvsyst.com/help/. Accessed 24. Nov. 2017.

[Quaschning, 2010] Quaschning, V. (2010). *Understanding renewable energy systems*. Earthscan.

[Rolls-Royce plc, 2017a] Rolls-Royce plc (2017a). Diesel and gas engines.

[Rolls-Royce plc, 2017b] Rolls-Royce plc (2017b). Marine Products and Systems.

[Rolls-Royce plc, 2018] Rolls-Royce plc (2018). About Marine. http://www.rolls-royce.com/products-and-services/marine/about-marine.aspx. Accessed 18. Mar. 2018.

[Ørsted, 2015] Ørsted (2015). DONG Energy acquires full control of one of the world's biggest offshore wind development zones. 21. Aug. 2015. http://hornseaprojectone.co.uk/News/2015/08/DONG-Energy-acquires-full-control. Accessed 26. Mar. 2018.

[Ørsted, 2018] Ørsted (2018). Ørsted UK fast facts. https://orsted.co.uk/Media/Press-kit/Fast-facts. Accessed 26. Mar. 2018.

[Saw et al., 2017] Saw, M. H., Khoo, Y. S., Singh, J. P., and Wang, Y. (2017). Enhancing optical performance of bifacial PV modules. *Energy Procedia*, 124:484–494.

[Ship & Bunker, 2018] Ship & Bunker (2018). Global Average Bunker Price. Last updated 28. Mar. 2018. https://shipandbunker.com/prices/av/global/av-glb-global-average-bunker-price#MGO. Accessed 28. Mar. 2018.

[Smith et al., 2015] Smith et al. (2015). Third IMO Greenhouse Gas Study 2014.

[Solanki, 2015] Solanki, C. S. (2015). *Solar Photovoltaics: fundamentals, technologies and applications*. Prentice-Hall of India, third edition.

[S&P Global Platts, 2017] S&P Global Platts (2017). LNG industry conversion.

[Statistics Norway, 2018] Statistics Norway (2018). Kjørelengder. Published 27. Apr. 2018. https://www.ssb.no/klreg. Accessed 19. May 2018.

[Østensjø Rederi, 2018] Østensjø Rederi (2018). Edda Passat. http://ostensjo.no/fleet/eddapassat/. Accessed 26. Mar. 2018.

[Stensvold, 2015] Stensvold, T. (2015). Denne fergen er revolusjonerende. Men passasjerene merker det knapt. Teknisk Ukeblad. https://www.tu.no/artikler/denne-fergen-er-revolusjonerende-men-passasjerene-merker-det-knapt/222522. Accessed 14. Apr. 2018.

[Stuards, 2015] Stuards, M. (2015). First in the World Electric Car Ferry Enters Service. Published 19. May 2015. https://www.vesselfinder.com/news/3421-First-in-the-World-Electric-Car-Ferry-Enters-Service-. Accessed 14. Apr. 2018.

[SunPower, 2016] SunPower (2016). SunPower E-Series Commercial Solar Panels | E20-435-COM.

[SunPower, 2018] SunPower (2018). Nearly Three Decades of Solar Leadership. https://global.sunpower.com/company/. Accessed 22. Jan. 2018.

[Tesla, 2018] Tesla (2018). Model S. https://www.tesla.com/models. Accessed 09. May 2018.

[The Research Council of Norway, 2018] The Research Council of Norway (2018). Large-scale programme for energy research (ENERGIX). https://www.forskningsradet.no/prognett-energix/Home_page/1253980140022. Accessed 10. May 2018.

[Transocean Coatings, 2018] Transocean Coatings (2018). Estimation of surface areas.